Published in final edited form as:
Neuroscience. 2010 July 28; 168(4): 982–1008. doi:10.1016/j.neuroscience.2009.10.028.

Molecular Disruptions of the Panglial Syncytium Block Potassium Siphoning and Axonal Saltatory Conduction: Pertinence to Neuromyelitis Optica and other Demyelinating Diseases of the Central Nervous System

John E. Rash, PhD
Department of Biomedical Sciences, Program in Neuronal Growth and Development, and Program in Cell and Molecular Biology, Colorado State University, Fort Collins, CO 80523

John E. Rash: john.rash@colostate.edu

Abstract

The panglial syncytium maintains ionic conditions required for normal neuronal electrical activity in the central nervous system (CNS). Vital among these homeostatic functions is "potassium siphoning", a process originally proposed to explain astrocytic sequestration and long-distance disposal of K^+ released from unmyelinated axons during each action potential. Fundamentally different, more efficient processes are required in myelinated axons, where axonal K^+ efflux occurs exclusively beneath and enclosed within the myelin sheath, precluding direct sequestration of K^+ by nearby astrocytes. Molecular mechanisms for entry of excess K^+ and obligatorily-associated osmotic water from axons into innermost myelin are not well characterized, whereas at the output end, axonally-derived K^+ and associated osmotic water are known to be expelled by Kir4.1 and aquaporin-4 channels concentrated in astrocyte endfeet that surround capillaries and that form the glia limitans. Between myelin (input end) and astrocyte endfeet (output end) is a vast network of astrocyte "intermediaries" that are strongly inter-linked, including with myelin, by abundant gap junctions that disperse excess K^+ and water throughout the panglial syncytium, thereby greatly reducing K^+-induced osmotic swelling of myelin. Here, I review original reports that established the concept of potassium siphoning in unmyelinated CNS axons, summarize recent revolutions in our understanding of K^+ efflux during axonal saltatory conduction, then describe additional components required by myelinated axons for a newly-described process of voltage-augmented "dynamic" potassium siphoning. If any of several molecular components of the panglial syncytium are compromised, K^+ siphoning is blocked, myelin is destroyed, and axonal saltatory conduction ceases. Thus, a common thread linking several CNS demyelinating diseases is the disruption of potassium siphoning/water transport within the panglial syncytium. Continued progress in molecular identification and subcellular mapping of glial ion and water channels will lead to a better understanding of demyelinating diseases of the CNS and to development of improved treatment regimens.

I. Introduction

Our lives depend on high-velocity, high-frequency propagation of axonal action potentials over long distances within the central nervous system (CNS) and peripheral nervous system (PNS). Local anesthetics, many neurotoxins, and diverse neurological diseases directly interfere with the molecules that underlie either neuronal synaptic transmission or axonal action potential propagation. However, recent studies have revealed that a wide variety of devastating neurological diseases result from genetic or autoimmune disruption of the intricate glial pathways that are specialized to support neuronal activity, particularly those glial mechanisms that provide for long-distance potassium siphoning and for transport and release of obligatorily-associated osmotic water.

This review describes an emerging model for understanding several demyelinating diseases of the CNS that derive from destruction of diverse molecular components of the panglial syncytium, but that are characterized by common features of blocked saltatory conduction associated with demyelination and the formation of sclerotic plaques. I first describe the cells of the panglial syncytium, then review the revolution that is occurring in our understanding of saltatory conduction, only recently recognized to be based on the spatial separation of ion pathways for sodium *vs.* potassium. With axonal sodium conductance localized to nodes of Ranvier, but potassium conductance now recognized to occur primarily enclosed within and isolated by the paranodal and internodal myelin layers[18,19,97,99] (detailed in **Sections V-VII**), concepts of the pathways for sequestration and intercellular transport of axonally-derived K^+ and obligatorily-associated osmotic water must be fundamentally revised. Therefore, I also review recently-discovered molecular sites of action of several genetic and autoimmune diseases that alter or destroy K^+ siphoning and associated co-transport of osmotic water, and as a consequence, disrupt saltatory conduction/axon signaling. Although each disease disrupts a different and discrete molecular locus in the panglial syncytium, all are characterized by reduced or blocked saltatory conduction caused by K^+-induced osmotic swelling of myelin, widespread segmental demyelination, and ultimately the formation of sclerotic plaques that typify many CNS demyelinating diseases, including specifically neuromyelitis optica[130] (NMO; also called “optico-spinal” or “Asian” multiple sclerosis [Asian MS]).

Finally, I present a new model of myelin disruption in NMO that is based on the recently-established immunological destruction of aquaporin-4 (AQP4) water channels at astrocyte endfeet, but whose cytotoxic effect is manifest at a distance as osmotic swelling and destruction of CNS myelin. The mechanism for producing this effect on myelin was not immediately apparent because myelin in the CNS is formed by oligodendrocytes and not the astrocytes that are the immediate target of immune destruction in NMO. I propose that with normal water efflux at astrocyte endfeet disrupted, excess water and K^+ are back-propagated through gap junctions between astrocytes and oligodendrocytes, as well as between successive, gap-junctionally-coupled myelin layers, causing oligodendrocyte myelin to become edematous, then sclerotic. Based on accumulating experimental and immunocytochemical data, the need is now clear to test new treatment approaches for NMO that minimize the excessive K^+/osmotic load that leads to secondary demyelination, and by blocking further damage, potentially to allow normal homeostatic mechanisms to repair damaged myelin. Moreover, with further damage to myelin blocked by suppression of the AQP4 immune response and by the use of “potassium-sparing” drugs, promising stem cell and other oligodendrocyte replacement technologies may then facilitate remyelination[2,132], thereby further restoring the capacity for saltatory conduction that is essential for normal CNS activity.

II. Cells of the panglial syncytium; who is coupled to whom?

The panglial syncytium (Fig. 1) is a vast network of interconnected glial cells, comprised of all three types of macroglial cells – astrocytes, oligodendrocytes, and ependymocytes – all of which are extensively inter-linked by gap junctions, with the highly-interconnected astrocytes serving as universal "intermediaries"[69]. The panglial syncytium pervades the CNS, where it provides widespread metabolic and osmotic support for neuronal somata, but it is particularly specialized for the ionic and osmotic homeostatic regulation of myelinated axons in white matter tracts.

The panglial syncytium consists of:

1. **Ependymocytes** (Fig. 1, *light blue*), the ciliated cells that line the brain ventricles and spinal canal. Ependymocytes contact cerebrospinal fluid and, thus, are potential sources and sinks for excess glial K^+ and H_2O. Ependymocytes are extensively linked to other ependymocytes by abundant homologous **E:E** gap junctions[17,22,50,69,102].
2. **Astrocyte**s (Fig. 1, *dark blue*), the most abundant cell of the CNS, are extensively coupled to other astrocytes (**A:A**) throughout the brain, optic nerve, and spinal cord via thousands of gap junctions per astrocyte[17,22,50,69], forming a "functional syncytium"[69]. Astrocytes are also extensively coupled to ependymocytes[102] by heterologous **A:E** gap junctions[69,102].
3. **Oligodendrocytes** (Fig. 1, *green*), the myelin forming cells of the CNS, are also extensively coupled to astrocytes (**O:A**), forming heterologous gap junctions on the outer surface of myelin, on everted paranodal loops[55], on oligodendrocyte somata, and on the "oligodendrite" processes that link each oligodendrocyte soma to as many as 20-60 different myelin segments[61; 91]. Initially, adjacent oligodendrocytes were also reported to be dye- or tracer-coupled[90], originally thought to imply the existence of homologous O:O gap junctions. However, ultrastructural analysis revealed that gap junctions do not directly link adjacent oligodendrocytes[45,69,102,106].

Instead, interposed astrocyte processes form concatenated gap junctions between closely adjacent oligodendrocytes[23,46] (Fig. 1, center), potentially providing a secondary pathway for aqueous, ionic, and tracer coupling of nearby oligodendrocytes. More important, abundant O:A gap junctions directly link oligodendrocytes and their myelin sheaths to surrounding astrocytes, thereby strongly linking them into the broader panglial syncytium[69,102]. Consequently, multiple segments of myelin (and their inter-connecting oligodendritic processes and somata) represent "tributaries" that converge on and feed excess K^+ and osmotic water directly into the astrocyte syncytium, thereby forming the osmotic and ionic "headwaters" of the panglial syncytium, with ultimate downstream release of K^+ and water via astrocyte endfeet at capillaries and the glia limitans.

In contrast, each segment of myelin in the PNS is formed by a separate Schwann cell. These cells are not gap junctionally-linked to other cells, and thus, do not possess an analogous conduit system for long-distance K^+ siphoning. Moreover, because peripheral nerves are not confined within the rigid encasement of the cranium or vertebral canal, cellular edema, myelin swelling, and sclerosis do not cause local compression of neuronal somata. Finally, even when damaged by sclerosis, PNS axons, unlike CNS axons, are able to regenerate, and the residual Schwann cells are able to remyelinate regenerating axons, as occurs during Wallerian degeneration and succeeding axon regeneration. Therefore, in this review, I have excluded discussion of mechanisms for the short-range dispersal of K^+ and water that occurs in the Schwann cells of the PNS, or of mechanisms leading to myelin degeneration in the PNS.

III. Potassium homeostasis in the CNS: Maintenance of low external potassium ion concentration (low $[K^+]_O$) required for normal neuronal activity

In the CNS, extracellular K^+ concentration ($\mathbf{[K^+]_O}$) is tightly regulated to *ca.* 2 or 3 mM, with normal axonal activity disrupted by even small increases in $[K^+]_O$. For example, increasing $[K^+]_O$ to 4 or 5 mM [*i.e.*, to *ca.* 3-4% of the normal 135 mM intracellular K^+ concentration ($\mathbf{[K^+]_I}$)] causes axonal depolarization and results in repetitive axon firing[48,124]. When $[K^+]_O$ is raised slightly further, to *ca.* 6 mM (*i.e.*, to only 4% of $[K^+]_I$), axonal conduction is blocked due to continuous inactivation of the voltage-gated Na^+ channels that are concentrated at the axon hillock and nodes of Ranvier[40,42,43]. Recent evidence suggests that to maintain low $[K^+]_O$ near these electrically-excitable portions of myelinated axons, particularly in large bundles of myelinated axons in the brain, spinal cord and optic nerve, higher vertebrates have evolved an efficient, highly-interconnected internal conduit system (*i.e.*, the panglial syncytium) that functions to: ***a)*** sequester axonally-derived K^+ and its associated osmotic water, ***b)*** transport both K^+ and water over long distances, away from the K^+-sensitive nodes of Ranvier, and ***c)*** dispose of this excess K^+ and accompanying osmotic water across astrocyte endfeet into capillaries or into the subpial space. Based on these new understandings of the role of the panglial syncytium in ionic and osmotic homeostasis, it is now possible to begin to understand how local release of K^+ during normal axonal saltatory conduction, restricted to the juxtaparanodal axolemma (described in **Section VI**), must be efficiently transported away to prevent localized myelin swelling, necrosis, and sclerosis.

IV. Potassium siphoning: Discovery and initial characterization

In their pioneering 1966 study, Orkand et al.[85] used a dissected optic nerve preparation from *Necturus* (a cold-blooded animal, which allowed multi-hour recording from its dissected axons) to document long-distance movement of K^+ immediately following each nerve stimulation. They showed that following low-frequency (0.5 Hz) stimulation of axons in the retinal end of the cut optic nerve, each compound action potential caused a 1-2 mV depolarization (Fig. 2A, *small arrow*) of astrocytes at the opposite end of the nerve bundle, up to several millimeters distant from the stimulating electrode (*i.e.*, several times the distance spanned by one astrocyte). At higher stimulation frequencies (>5 Hz), the K^+ potentials in those distant astrocytes fused and approached a plateau of +17 mV depolarization (Fig. 2A, *large arrow*). Thus, they suggested that the excess K^+ released during axonal activity entered and depolarized nearby astrocytes, whereupon it was rapidly transported away by an unknown mechanism, which nevertheless, caused the recorded strong depolarizations of distant astrocytes. (Neither gap junctions nor direct astrocyte coupling were known at that time.) Because the axons of *Necturus* optic nerve are unmyelinated, K^+ efflux from unmyelinated axons necessarily occurred directly into the peri-axonal extracellular space. Thus, depolarization of distant astrocytes implied that much of the axonally-released K^+ was absorbed directly into the abundant astrocyte processes that surround each axon. However, because K^+ efflux in myelinated axons occurs in a protected compartment beneath myelin (**Section VII**), it now appears inappropriate for others to have applied the Orkand model of K^+ siphoning/"K^+ spatial buffering" to myelinated axons. Consequently, this review presents a significantly revised model for K^+ siphoning that also incorporates the unique K^+ conductance properties of the myelinated axons in the CNS of higher vertebrates (**Section XVI**).

A. Astrocyte K^+ "leak" conductance is concentrated in astrocyte endfeet

Two decades after the pioneering studies of Orkand[85], Newman et al.[81,82] used intracellular recordings from the somata of astrocytes freshly dissociated from *Necturus* optic nerve, combined with focal iontophoresis of K^+, to show that K^+ "leak" conductances were highest

in the astrocyte endfoot processes (Fig. 2B, *traces a, b, g, h*) but were minimal at the astrocyte soma and its proximal processes (Fig. 2B, *traces c-f*). These localized differences in K^+ leak conductances implied that astrocyte somata had very few K^+ leak channels, but that their distal endfoot processes had densely packed K^+ leak channels. The molecular basis for this localization of K^+ leak conductance to astrocyte endfeet remained unknown for another decade.

B. K^+ efflux during saltatory conduction incorrectly localized to nodes of Ranvier

Until very recently, it was widely believed that during saltatory conduction, both Na^+ and K^+ conductances occurred intermixed within the nodal plasma membranes at nodes of Ranvier in both CNS and PNS axons (Fig. 2C), but with K^+ conductance occurring *ca.* 1 msec after Na^+ conductance (*i.e.*, "temporal separation" rather than "spatial separation" of conductances; Fig. 2C, *bottom left*). Consequently, virtually all physiology textbooks and many experimental studies continue to account for saltatory conduction based on this incorrect model.

C. Astrocytes near nodes do not sequester K^+ from the nodal extracellular space

One major erroneous assumption regarding potential K^+ siphoning in myelinated axons of the CNS was that astrocyte processes near nodes of Ranvier effectively sequester the K^+ that was presumed to be released into the nodal extracellular space, similar to that proposed for the unmyelinated axons of *Necturus* optic nerve. This presumption appeared to be supported by early freeze-fracture electron micrographs of myelinated axons in higher vertebrates [Fig. 2D, from126], which showed astrocyte processes in close proximity to nodes of Ranvier (*eA2* in Fig. 2D1*; eA* in Fig. 2D2). This close anatomical relationship was widely assumed to allow potassium siphoning directly into astrocytes near myelinated axons, similar to that found in *Necturus* optic nerve. However, this model of saltatory conduction and K^+ siphoning had a major flaw: During repetitive saltatory conduction, there was no detectable increase in external K^+ at or near nodes of Ranvier[24]. That observation strongly contradicted previous models because it suggested: *a)* that there were no voltage-gated K^+ channels (Kv1 channels) within the nodes of Ranvier through which K^+ conductance could occur; and therefore, *b)* that K^+ released during saltatory conduction could not enter "nodal" astrocytes. Several lines of evidence[24,113] quickly revealed that, following pathological detachment of the paranodal loops of myelin from the nodal plasma membrane, either: *a)* by enzymatic or by lysolecithin digestion, *b)* in demyelinating diabetic neuropathy, or *c)* following exposure of axons to diphtheria toxin, axonal K^+ efflux became directly detectable for the first time near nodes of Ranvier. Those results provided an important clue that K^+ efflux during normal saltatory conduction does not occur at nodes of Ranvier, but rather, occurs in the internodal region, under the myelin sheath, where axonal K^+ conductance is normally isolated from the recording electrodes by paranodal axo-glial septate junctions and by the high-resistance interlammelar myelin tight junctions[14,108]. Unfortunately, the significance of this observation regarding K^+ conductance in the internodal region remained unrecognized for another decade.

D. Directionality of potassium siphoning/potassium spatial buffering

The directionality of K^+ and water flow has been inferred from two primary observations:

1. The distal (output) end of the syncytial pathway is formed by specialized astrocyte endfoot processes that release copious amounts of neuronally-derived K^+ and associated osmotic water, either into the peri-capillary space of blood vessels that perfuse the parenchyma of the brain and spinal cord (Fig. 1, paired *blue* and *red arrows*) or into the subpial space that surrounds the brain and spinal cord[70-72,83,107] (Fig. 1, right side).

2. K^+ derived from axons during saltatory conduction is first detected in innermost myelin[28,29] (**Section V**). However, structural pathways for K^+ and water entry into

the panglial syncytium are not well characterized at the molecular level. Thus, the precise molecular pathways for entry of K^+ and water into the panglial syncytium are now under intense scrutiny.

V. Emerging role of myelin in K^+ siphoning

The development and use of ultra-sharp electrodes[28,29] to penetrate and measure electrical potential in successively deeper myelin layers (Fig. 2E) provided new insights into the physiology of saltatory conduction. David et al.29 showed that following each action potential, the innermost "peri-internodal compartment" depolarized to as high as +75 mV following high-frequency axonal stimulation. This was a major surprise because no existing model could account for a positive electrical potential of this magnitude, either intracellularly within myelin or extracellularly between the myelin internodal interlammelar spaces, which are minimal in compact myelin (but see Fig. 6-10 in Peters et al[91] suggesting an approximate 10-nm interlamellar space, bridged by stacked tight junctions). Moreover, because of limited resolution of confocal microscopy, it was not possible in that early report29 to determine whether the peri-internodal compartment corresponded to the extracellular space between the axon and the myelin sheath or to the innermost cytoplasmic layer of myelin. This distinction may be important because it is not yet determined whether K^+ arising from saltatory conduction is:

- **a.** released from axons directly into the extracellular peri-axonal space within each myelin segment,
- **b.** occurs through trans-cellular ion channels, directly from axonal cytoplasm into the innermost layer of cytoplasmic myelin (potential mechanisms described in **Section VI**), or
- **c.** occurs via both mechanisms, but each occurring separately under low *vs.* high stimulation frequencies (*i.e.,* condition "a", above, *vs.* condition "b").

To begin to address this issue, David and coworkers showed that iontophoresis of K^+ into the peri-internodal compartment (Fig. 2E, *lower trace*) mimicked the extreme voltage changes recorded after normal axonal activity (*i.e.,* to as high as +75mV). This iontophoretic manipulation of peri-internodal voltage suggested that axonal K^+ efflux occurred into an electrically-isolated compartment, where peri-internodal K^+ concentration (**$[K^+]_P$**) was elevated up to 100 mM for up to several hundred milliseconds after high-frequency stimulation (*i.e.,* to 30-fold greater $[K^+]_O$ than in normal CSF), approaching but not quite reaching normal intracellular concentrations (*i.e., ca.* 130 mM; Fig. 2E; $[K^+]_P$; calibration bars at *upper left*). Moreover, this excess K^+ within the peri-internodal space did not rapidly return to the axon, suggesting either: ***a)*** that there are few K^+ leak channels and/or few Na^+/K^+ ATPase molecules in the axonal internodal plasma membrane to rapidly lower $[K^+]_P$, or ***b)*** that the increased K^+ in the peri-internodal compartment was not in the extracellular space, but instead, was in the innermost layer of cytoplasmic myelin, pending trans-lamellar transport to the outer layers of myelin. (For potential mechanisms, see **Section XVI.**)

VI. Structure, function, and composition of nodes of Ranvier, paranodes, and juxtaparanodes

By 2002, Rasband, Scherer, Brophy, Levinson, Trimmer, Rosenbluth, Ellisman, and others had used a battery of antibodies for simultaneous demonstration that:

- **a.** **v**oltage-gated Na^+ channels (**Nav1** family) were localized exclusively within the axonal plasma membrane at nodes of Ranvier (Fig. 3A, *green fluorescence*), whereas

b. **v**oltage-gated K^+ channels (**Kv1** family) were not co-localized at nodes of Ranvier as commonly believed, but instead, were localized to the internodal axonal plasma membrane, concentrated entirely beneath juxtaparanodal[93,97,125] and internodal myelin (Fig. 3A, *blue fluorescence*), including in a thin line that followed the inner mesaxon from juxtaparanode to juxtaparanode (Fig. 3B1). This linear distribution of Kv1 channels along the inner mesaxon was beautifully documented in PNS axons (Fig. 3B1,2) but was only weakly discernable in the much smaller CNS axons of the optic nerve (Fig. 3B3,4). Interposed between voltage-gated Nav1 and Kv1 channels were:

c. contactin and contactin-associated protein (**caspr;** Fig. 3A, *red fluorescence*), which are two primary components of the septate or septate-like junctions* (Fig. 3C2; *arrows*; also see Section VII), the points at which paranodal loops contact the axonal plasma membrane and form strong diffusion barriers between the nodal extracellular space and the peri-internodal space[6,18,97,98,108] (Fig. 3D, *red band*). Rosenbluth, Bhat, and co-workers showed that both contactin and caspr were essential for maintaining a 1-2 μm spatial and electrical segregation of voltage-gated Na^+ channels of nodal plasma membranes from voltage-gated K^+ channels of the juxtaparanodal plasma membrane[14,108] (Figs. 3B2,B4). They then documented that after caspr/contactin knockout, Kv1 channels drifted from juxtaparanodes to close to the nodes (Fig. 3B4), but did not intermix with Nav1 channels. They also showed that under these conditions, saltatory conduction ceased when the neurexin/contactin/caspr-paranodin barrier was disrupted[14], even though both Nav1 and Kv1 channels were still present at normal densities. This demonstrated that electrical isolation of Na^+ *vs.* K^+ conductances by the septate junctions, and not simply their spatial segregation, was essential for the process of saltatory conduction.

Based on the demonstration that axonal K^+ efflux occurs into the protected and isolated peri-internodal compartment[29], this means that astrocyte fingers that are normally found near nodes of Ranvier, and therefore are outside the peri-internodal compartment, CANNOT BE exposed to increased K^+ in the extracellular space around nodes (Fig. 2D; shown diagrammatically as Fig. 3D, below the dashed line). Although not explicitly stated, this observation effectively eliminated the previously-assumed entry point for axonal K^+ into the astrocyte syncytium during potassium siphoning. It also required the existence of a previously unsuspected route for K^+ siphoning, initially into internodal myelin before entering the astrocyte syncytium (**Sections VI and XVI**).

A. Proposed structural pathway for K^+ in the juxtaparanodal axon plasma membranes

More than 30 years ago, freeze-fracture replicas of myelinated axons in the PNS revealed abundant “rosettes” of intramembrane particles (**IMPs**) in the external membrane leaflet (**E-face**) of the juxtaparanodal axon plasma membrane (Fig. 4A and inset), as well as in a thin strip running along the inner mesaxon from juxtaparanode to juxtaparanode[67,117,118], precisely where K^+ conductance/voltage-gated Kv1 channels were subsequently shown to occur in abundance (Fig. 4C2; from1). This suggested even then that the axonal rosettes might have an unrecognized role in saltatory conduction, possibly corresponding to voltage-gated K^+ channels118. Equally important, the same freeze-fracture replicas67,117,118 revealed that the

*Septate junctions, as originally defined, are intercellular junctions between glial cells of insects, where their primary protein, Neurexin-IV[12], is evolutionarily homologous to contactin in vertebrate septate-like junctions[6,16,31]. Despite the similarity of function and molecular homology, many investigators insist that the paranodal junctions at nodes of Ranvier be called “septate-like junctions”[31] rather than septate junctions. However, I note that other functionally-related intercellular junctions (*e.g.*, invertebrate *vs.* vertebrate gap junctions) are given the same name even though these gap junctions are composed of non-homologous proteins (innexins vs. connexins). In contrast, invertebrate septate junctions and vertebrate septate-like junctions are similar in structure and are composed of homologous proteins. Thus, in this review, I refer to these ubiquitous diffusion barriers as septate junctions.

innermost (adaxonal) layer of Schwann cell myelin membrane overlying the juxtaparanodal axonal plasma membrane also contained distinctive rosettes of **P-face** (protoplasmic leaflet) particles (Figs. 4B1,B2, *arrowheads*) of exactly the same spacing as the axonal E-face particle rosettes (Figs. 4B1, *arrowheads;* **B3**, *large arrow*). On rare occasions, the fracture plane stepped from axonal to Schwann cell plasma membranes within an individual rosette (Fig. 4B3, *large arrow*), revealing that the axonal E-face particles were precisely aligned with the particles in the P-face rosettes in the myelin plasma membrane[117], demonstrating structural coupling and, therefore, implying functional coupling of the two distinct types of rosette particles. Thus, Stolinski et al.[117,118] presciently speculated that the axonal rosettes might represent voltage-gated K^+ channels – a conjecture that has yet to be validated. They further speculated that the closely-associated myelin rosettes might represent unidentified channels for metabolic or ionic communication between the axon cytoplasm and the innermost cytoplasmic layer of Schwann cell myelin (*i.e.*, properties of gap junction channels). Regardless, the functions of the axonal E-face particle rosettes and the myelin P-face rosettes remained unknown and unexplored for more than 30 years, pending development of high-resolution electron microscopic immunocytochemical labeling methods.

B. Connexin29 (Cx29) co-localized with Kv1 channels

Cx29 (connexin of 29 kDa) is expressed in both oligodendrocytes and Schwann cells, but unlike other connexins, Cx29 does not form gap junctions1,75 (next paragraph). This may indicate that Cx29 has been co-opted for a different but related function. By immunofluorescence microscopy, both Cx29 and Kv1 channels are closely co-localized within juxtaparanodes, and more remarkably, narrowly follow the inner mesaxon in myelinated axons in both CNS and PNS (Fig. 4C)[3].

C. Cx29 identified in adaxonal myelin P-face rosettes; connexon hemichannels *vs*. coupled ion channels

SDS-FRL[35,36] and freeze-fracture replica immunogold labeling (**FRIL**104,106; derived from SDS-FRL and confocal "grid-mapped" freeze fracture101,102) are high-resolution immunocytochemical methods for biochemical analysis of subcellular structures at the ultrastructural levels, with FRIL having the added advantage of allowing confocal grid-mapping of immunocytochemically-identified structures, from the gross anatomical and histological levels to the ultrastructural and macromolecular levels. FRIL analysis of myelinated axons in sciatic nerve revealed that the P-face particle rosettes in the adaxonal layer of Schwann cell myelin[57] (Fig. 4D), including those that were tightly clustered in Schwann cell juxtaparanodal membranes[57], were immunogold-labeled for Cx29. Because no connexin coupling partner for Cx29 has been identified in the axonal plasma membrane[1,3], one possibility is that Cx29 rosette IMPs represent unpaired Cx29 "hemichannels". The structural coupling of Cx29 IMPs to the axonal E-face rosette IMPs is equally confusing because no connexin is found as E-face particles in any membrane. Interestingly, innexins (invertebrate connexins; homologous to pannexins; **Section VIIA**) form gap junctions in invertebrates that consist of E-face particles (rather than the P-face particles that comprise vertebrate gap junctions), potentially suggesting an innexin/pannexin coupling partner for Cx29. However, a more likely structural and functional coupling partner for the Cx29 rosettes are the abundant Kv1 channels that are concentrated in the same area (Fig. 4C2).

VII. Nodes of Ranvier in the CNS: dual axonal and glial functions

It is well established that in the CNS of higher vertebrates, oligodendrocytes form multiple sheet-like cytoplasmic processes that spiral around axons and then compact to form the mature myelin sheaths. Because of their distinctive appearance by light microscopy, the unmyelinated spaces between successive myelin segments, as delineated by closely adjacent myelin

swellings, were designated axonal "nodes" by Louise-Antoine Ranvier in 1871[96]. However, these nodes of Ranvier are more properly defined, not by their absence of myelin, but instead, by the molecular specializations and compositions of the axon nodal plasma membrane and of the membranes of its essential glial co-participants[7,14,108,129].

A. Glial specializations at the node of Ranvier

The composite node of Ranvier is characterized and delineated by the most complex and elaborate intercellular junctional complex in all biology, involving three different cell types (neurons, astrocytes, and oligodendrocytes) that form multiply-redundant intercellular appositions that utilize four different types of intercellular junctions to regulate and augment saltatory conduction in CNS axons:

1. Septate junctions (Fig. 5 and inset, *red triplet IMPs*), which are at the edge of the myelin sheet, bind the non-compact paranodal loops of myelin to the axonal plasma membrane, forming a continuous spiral diffusion barrier (Fig. 5; *red spiral around axon*, lower left and right; enlarged in *inset*, lower right) that separates the internodal peri-axonal space (*P*) from the nodal extracellular space (*N*). These multi-stranded diffusion barriers efficiently compartmentalize and isolate the axonally-released K^+ from the K^+-sensitive node of Ranvier.

2. Tight junctions, arranged in multiple parallel strands (Fig. 6), link the innermost abaxonal and adaxonal layers of cytoplasmic internodal myelin (Fig. 5, *triple line of brown diamonds*), as well as each successively more external layer of compact myelin. These complex tight junctions strands run continuously from one paranode to the next[64,69] (Fig. 6A,B), forming multiple isolated extracellular compartments, one per turn, within internodal myelin. Thus, the internodal myelin intralamellar compartments are separated by strong interlamellar tight junction barriers that further prevent circumferential diffusion of K^+ and water from the internodal "peri-axonal space" (*P*) into the space between successive myelin layers (*numbered compartments*) or into the peri-nodal extracellular space (*N*). Additional circumferential tight junction strands[45] link successive paranodal loops of myelin (Fig. 5, *left end* and *right end*; Fig. 7D1,D3), further isolating these interlamellar compartments from the extra-nodal space.

3. Autologous (interlamellar) gap junctions couple successive cytoplasmic layers of paranodal myelin (Fig. 5, *green IMP clusters* indicated by *brackets*; also Figs. 7D1,D2, D4,D5). These gap junctions provide direct trans-lamellar pathways for ions and water, thereby ionically, osmotically, and electrically linking the innermost to the outermost layers of cytoplasmic paranodal myelin[45,66]. Paranodal gap junctions are composed of a single ("homotypic") connexin protein (Cx32), making this essential pathway particularly susceptible to genetic disease (**Section XIII**).

4. Heterologous (intercellular) gap junctions couple the outermost cytoplasmic layer(s) of myelin to abutting astrocyte processes forming oligodendrocyte/astrocyte (**O:A**) gap junctions (Fig. 5, *green IMP clusters* on outermost layer of myelin, including everted paranodal loops; Fig. 8C). These **O:A** gap junctions, are composed of four or five different connexin proteins (*i.e.*, they are "heterotypic"; **Section VIII**), which not only imparts special conductance properties to these junctions[87], but this redundancy of connexin expression also seems to insure their continued functionality should any one of their five connexin genes be mutated. (Myelin disrupting diseases resulting from mutations of glial connexins are described in **Sections XIII** and **XV.**)

VIII. Gap junctions of the panglial syncytium

A. General considerations

In all vertebrate species, gap junctions are tight aggregates of a few transmembrane channels ("connexons") to tens of thousands of connexons. Within each gap junction, individual connexons pair and link across the extracellular space to form leakless pathways between the cytoplasms of coupled cells. In vertebrate species, gap junctions provide for direct intercellular diffusion of ions, water, and small globular molecules up to about 500 mw[44]. In each of two coupled cells, gap junction hemiplaques are composed of from one to as many as three of the 20 or 21 different connexin proteins114 identified in the mouse and human genomes †. Current evidence suggests that in most gap junctions *in vivo*, six identical connexin molecules assemble like barrel staves to form a "homomeric" connexon hemichannel. Although it is theoretically possible that two different connexins can assemble to form a "heteromeric" connexon, there is as yet no direct evidence for heteromeric connexons *in vivo* in any cells of the CNS.

In coupled cells of the same histological type (*i.e.*, homologous coupling), homomeric connexons may link to similar homomeric channels in the second cell, forming "homotypic" channels[56]. In contrast, gap junctions formed between unlike cells (heterologous couplings) may consist either of identical homomeric connexons, forming homotypic channels (*e.g.*, Cx43:Cx43, as in E:A gap junctions), or they may assemble from unlike homomeric connexons, forming heterotypic channels (*e.g.*, Cx47:Cx4345,[56]; as in O:A gap junctions). Moreover, many cell types express two or more connexins[26], and when these like cells couple, they may form bi- or tri-homotypic gap junctions[56]. Similarly, unlike cells, each expressing two or more connexins may also form bi- or tri-heterotypic gap junctions[56]. All of these potential configurations occur in the panglial syncytium, and as documented below, each connexin pairing combination uniquely contributes to the process of voltage-augmented dynamic K^+ siphoning that is associated with myelinated axons.

A. Cell-specificity of connexin expression

1. Ependymocyte connexins—By immunofluorescence microscopy and by FRIL, gap junctions between adjacent ependymocytes consist of Cx43 in both apposed hemiplaques[102-104], with no other connexin identified in these gap junctions. In addition, FRIL data suggest that gap junctions between ependymocytes and astrocytes contain Cx43 on both sides but apparently do not contain any other connexin (*i.e.*, these heterologous couplings are homotypic)[103,107].

2. Astrocyte connexins—Astrocytes express three connexins – Cx43, Cx30, and Cx26 (listed in order of decreasing abundance). Thin-section electron microscopic immunolabeling[133-135] and FRIL[73,78,106] revealed that both Cx43 and Cx30 usually occurred in both apposed hemiplaques of A:A gap junctions (Figs. 7B, 8C1,C2). Cx43 along with Cx30 and Cx26 were found by double labeling of A:A and O:A gap junctions, particularly in white matter tracts of the CNS[75,77,105]. Cx43 homotypically couples to Cx43 but not to Cx30; Cx30 couples to Cx30; and Cx26 couples to Cx26[4,75]. Homologous **A:A** gap junctions are composed of two principal connexins (Cx43 and Cx30)[49,75-78,84,105,134], plus in limited

† In invertebrate species, including insects and mollusks, gap junctions are composed of non-homologous proteins called "innexins" (*in*vertebrate con*nexins*"), which allow permeation of slightly larger molecules than vertebrate gap junctions (1000-1400 mw[58] *vs. ca.* 500 mw44). Recently, three homologous innexin-like genes were found in the human genome and designated "pannexins" [pan-specific innexins][10,11,20,88,89]. Px-1 and Px-2 are found in the vertebrate CNS, but to date, pannexin proteins have not been demonstrated in any gap junction in any vertebrate species, and their localization, ultrastructural configurations, and functions remain unknown. However, Px-1 and Px-2 have been proposed to represent functional "hemichannels" that release ATP, Ca^{++}, and small molecules into the extracellular space[122]. To date, there is no evidence that pannexins have intercellular interactions with any other transmembrane channels.

areas of the CNS, an additional minor connexin (Cx26[4,75,77,105]; but see34), forming bi- or tri-homotypic gap junctions[4,47,86].

3. Oligodendrocyte connexins—Oligodendrocytes express their own unique set of three connexins: Cx47, Cx32 and Cx29[3,45,47,74,75]. Cx32 was the first oligodendrocyte connexin to be identified unambiguously[109]. Cx32 has been documented immediately adjacent to nodes of Ranvier (Fig. 7A), on oligodendrocyte somata (Fig. 7B; from[45]; Fig. 8B from54), and on their cytoplasmic processes ("oligodendrites")[54]. Cx32 is present in both CNS myelin45 and PNS myelin9,64, where from dye coupling experiments and from immunofluorescence labeling, Cx32 was proposed to link successive myelin layers, both at Schmidt-Lanterman incisures[64] and paranodal loops of myelin[103]. Cx47, originally misidentified as a neuronal connexin[120], was subsequently documented only in oligodendrocyte gap junctions[55]. Cx29, the third oligodendrocyte connexin, does not form gap junctions, and its roles remain unresolved, but it may have a role in K^+ siphoning (**Section IV.C**).

a. Gap junctions linking successive myelin lamellae at paranodes consist of Cx32, only: Immunofluorescence labeling using antibodies to caspr as a marker for paranodes (Figs. 7A1,A3; *green fluorescence*) and antibodies against Cx32 (Figs. 7A2,A3; *red fluorescence*) revealed both small puncta and linear immunofluorescent bands co-localized with caspr in the paranodal region of myelinated fibers (Fig. 7A3). Although it was presumed that the puncta represented gap junctions, the limits of resolution of confocal microscopy did not allow determination of whether the puncta were between myelin layers or were on the outer surface of myelin, nor did confocal microscopy allow determination of the size or configuration of the putative gap junctions.

By FRIL, Cx32 was demonstrated at ultrastructurally-defined gap junctions between successive myelin layers at paranodes, forming "autologous" or "reflexive" gap junctions[45,52,55]. These paranodal gap junctions often consisted of unusual linear ("string") configurations (Figs. 7D2,D4,D5), as well as small plaques[103]. String gap junctions were distinguished from superficially similar tight junctions (Fig. 7D3) based not only on the different antibodies that labeled the two types of junctions[55], but also on the distinctively different cleaving patterns of these two types of junctions45. Thus, with respect to Cx32 in paranodal gap junctions, CNS myelin is similar to PNS myelin, wherein Cx32 immunofluorescence[9,109,110] and gap junctions containing Cx32 (but no other connexins) are found between successive layers of myelin[64]. In contrast, Cx47 was not detected in interlamellar gap junctions. Based on this expression of a single connexin at interlamellar paranodal gap junctions, mutation or knockout of Cx32 would be expected to have major consequences for the functions of paranodal myelin (**Section XIIIA**).

b. Oligodendrocyte hemiplaques at O:A gap junctions usually contain abundant Cx47: Recently, Cx47 was identified as the second connexin in oligodendrocyte gap junctions[66], and it quickly became evident that Cx47 is by far the most abundant in gap junctions on oligodendrocyte somata, proximal processes, and on the outer surface of myelin[55]. By confocal microscopy, oligodendrocyte Cx47 immunofluorescence (Fig. 8A3) was always co-localized with equally abundant Cx43, particularly at paranodes (Fig. 8A) and somata (Fig. 8B).

By FRIL, Cx47 was almost always co-localized with Cx32 on the oligodendrocyte-side of O:A gap junctions (Fig. 8B1,2), where immunogold labeling for Cx47 was often 5-10 times as great as for Cx32[55]. In some cases, only Cx47 was found in O:A junctions, without Cx32[45]. Because oligodendrocyte Cx32 is unable to couple to astrocyte Cx43, and oligodendrocyte Cx47 is unable to couple with astrocyte Cx30[4,33,127,128]; and because the relative amounts of Cx47 parallel those of Cx43, and Cx32 parallels the amount and distribution of Cx30 at O:A gap junctions, functional coupling combinations at O:A gap junctions are now known to be

Cx47:Cx43 and Cx32:Cx30[4,47,86]. This cell-type-specific expression of connexins and the differential subcellular distributions of different connexins in oligodendrocytes and astrocytes have important ramifications for connexin diseases of glia, particularly connexin mutations and genetic knockouts that interfere with K^+ siphoning and water transport (**Sections XIIIA-C**, **XV**).

D. Connexins in oligodendrocyte coupling partners: The astrocyte connection

Oligodendrocytes form intercellular gap junctions only with astrocytes (O:A) and not with other oligodendrocytes[60,69,102,106] (Figs. 7B,C; diagrammed in Fig. 5), and these gap junctions were labeled for Cx32 and/or Cx47 (Figs. 7B,C, 8B) but no other connexins. In freeze-fracture replicas, the cellular coupling partners for these oligodendrocytes were readily identified as astrocytes by the presence of P-face AQP4 "square arrays" or E-face imprints of AQP4 arrays[51,60,102] (Fig. 7C, *yellow arrow*) or by their high density of other classes of non-aggregated IMPs in both E- and P-faces (Fig. 7C, *blue overlay*). In contrast, oligodendrocytes were identified by their large clear areas of membrane that are essentially devoid of both E-face and P-face particles (Fig. 7C, upper right; also see Figs. 7D2-D5, Fig. 8C1,C2, *right side*).

FRIL views from within oligodendrocytes toward their cellular coupling partners revealed labeling for connexins that are only in astrocytes, including Cx43 (Fig. 8C1), Cx43+Cx30 (Fig. 8C2), and Cx30+Cx26[75]. In images containing both cross-fractured myelin and outermost E-face of surface-fractured myelin (Fig. 8C1, *E-arrow*), gap junctions labeled for Cx43 (*10-nm gold beads*) and Cx30 (*20-nm gold beads*) were consistently observed (Fig. 8C1, *blue overlay*), thereby confirming these as myelin O:A gap junctions, with both Cx43 and Cx30 in the underlying astrocyte coupling partner.

At O:A gap junctions, oligodendrocyte Cx32, when present, was always co-localized with astrocyte Cx30[45,75,106], consistent with formation of heterotypic Cx32:Cx30 connexons[86]. Thus O:A gap junctions are composed of Cx47 and Cx32 on the oligodendrocyte side coupling with Cx43, Cx30, and occasionally Cx26[75], on the astrocyte side. This means that to uncouple oligodendrocytes from astrocytes, the genes for both Cx32 and Cx47 must be deleted or inactivated (**Section XIII**). Otherwise coupling, albeit reduced, continues to occur if the gene for either Cx32 or Cx47 remains functional. Thus, this redundancy of connexin expression may be protective for these essential coupling pathways.

IX. Astrocyte endfoot K^+ efflux pathways during K^+ siphoning

K^+ permeates astrocyte plasma membranes through a variety of K^+-selective channels, including the Kir4.1 "leak" channels that are concentrated at astrocyte endfeet. (Additional K^+ leak channels in astrocytes include the KCNK (K2P) channels[39,139], but their relative abundances and subcellular locations are not yet determined.) Kir4.1 and AQP4 water channels are strongly co-localized at all membrane surfaces where K^+ siphoning has been documented, but with AQP4 labeling far more abundant than labeling for Kir4.1. In the retina[48], for example, Kir4.1 K^+ leak channels were detected in abundance by thin-section immunogold labeling of the Müller endfoot plasma membranes that abut the vitreal surface (Fig. 9A1, *black arrow;* from70). (Müller cells are modified astrocytes in the retina.) In consecutive ultrathin sections, even more abundant immunogold labels for AQP4 [Fig. 9A2, *white arrow*] were present, and thereby confirmed to be interspersed with labels for Kir4.1 (Fig. 9A1). Initially, it could not be determined whether these differences in labeling density reflected different labeling efficiencies of the two rabbit polyclonal antibodies, or if AQP4 channels vastly outnumbered Kir4.1 channels. Regardless, this close parallel distribution but greater abundance of AQP4 over Kir4.1 labeling implies that the efflux of osmotic water at astrocyte endfeet is an essential element in K^+ siphoning. With osmotic water molecules *ca.* 350 times as abundant as potassium

ions at normal intracellular concentrations (i.e., 55 M *vs.* 140 mM = 350:1) and *ca.* 20,000-30,000 times as abundant as potassium ions in the extracellular milieu (i.e., 55 M *vs.* 2-3 mM), to maintain tonicity of endfeet during K^+ efflux, at least 350 water molecules must be transported in parallel with each potassium ion, simply to maintain osmotic balance within the endfeet. This predicts the need for far greater numbers of AQP4 channels (presumably as reflected in the number of immunogold labels for AQP4) than for Kir4.1 channels (number of gold labels for Kir4.1). In contrast to AQP4 (**Section X**), the ultrastructural correlates for Kir4.1 and other K^+ channels have not yet been identified.

X. Water efflux pathways during K^+ siphoning

In conventional freeze-fracture replicas, astrocyte endfoot plasma membranes contain high concentrations of distinctive P-face "square arrays" of particles. [These arrays are also called "orthogonally arranged particles" (OAPs)80،123،131،136]. By FRIL, these densely-packed square arrays were immunogold labeled by antibodies against AQP4 (Fig. 9B1-3), thereby defining them as AQP4 arrays[104,107].

In subsequent investigations of possible assembly mechanisms for AQP4 into arrays, *in-vitro* expression systems revealed that the sizes of the AQP4 arrays were, in part, determined by the ratio of the two primary alternatively-spliced variants of AQP4, designated M1 and M23[79]. Translation of M1 begins at **m**ethionine in the first amino acid position (*i.e.*, aa1; designated M1), whereas translation of the M23 variant begins at the second methionine, which is aa23 in the gene sequence. Cells transfected with M23 (no endogenous M1) form large arrays with up to several hundred protein particles per array. Each large array was labeled multiple times for AQP4 (Fig. 9B3), confirming that the arrays are formed from AQP4 protein – in this case, the M23 variant. In contrast, cells transfected with cDNA for M1 do not form stable square arrays, but instead, had increased numbers of dispersed 6-nm IMPs[37]. Finally, cells transfected with both M1 and M23 formed numerous but mostly smaller arrays. These combined data suggested that the assembly state and possibly the functional state of the arrays is regulated by differential expression of these two primary splice variants. Recently, Suzuki et al.119 showed evidence that the M1 variant has two cysteine residues that are palmitoylated, with the attached lipid moiety proposed to interfere with array assembly, thereby regulating the sizes of the arrays, and possibly their functional state. However, that proposal for regulating AQP4 arrays has been challenged by Crane and Verkman27. In any case, the cellular and histological expressions of M1, M23, and the several other AQP4 variants[68،115] have not been determined in human or any other CNS tissues. Moreover, neither the assembly state nor the immunological destruction and removal of any of these AQP4 splice variants has been investigated during the progress of neuromyelitis optica (NMO), which was recently determined to be an autoimmune disease directed against AQP4 in astrocyte endfeet (**Section XVI**).

XI. Entry points for osmotic water into the panglial syncytium not yet identified

In their pioneering paper, Nagelhus and coworkers[72] used thin-section immunogold labeling to investigate possible entry points into the glial syncytium for the osmotic water that accompanies K^+ during K^+ siphoning. They showed that astrocyte membranes immediately adjacent to the nodes of Ranvier were essentially devoid of AQP4 water channels [Fig. 9D; from72], whereas astrocyte processes more distant from the nodes were enriched in labeling for AQP4 [Fig. 9D, *right side*]. This differential distribution showed that the near absence of AQP4 labels on processes immediately adjacent to nodes of Ranvier did not arise from labeling artifact, but instead reflected local differences in subcellular distribution of AQP4, suggesting that water does not enter the glial syncytium at those astrocyte processes that surround the

node. Although the entry point for water during potassium siphoning remains unknown, circumstantial evidence implicates the adaxonal myelin plasma membrane (**Section XIII**).

XII. Syncytial pathways for H_2O and K^+

Throughout the astrocyte syncytium, square arrays are frequently observed to be clustered in close proximity to gap junctions (Fig. 9E; *blue vs. red overlays*). FRIL confirmed that these arrays also contained AQP4 (Fig. 9E2,9E3). Near gap junctions, where apposed membranes are brought closer together, gold labels for AQP4 often were found beneath E-face images of square arrays. Because the E-face pits represent the imprints from which the AQP4 proteins had been removed, the protein-free E-face pits could not have been labeled directly. Therefore, the apparent immunogold labeling of E-face arrays was attributed to "cryptic" labeling of subjacent, aligned AQP4 arrays in the closely apposed astrocyte plasma membrane, much like the labeling observed beneath the E-face pits in nearby freeze-fractured gap junctions (Fig. 9E2), where such cryptic labeling is well established[36,104,106]. This stacked alignment of AQP4 arrays between closely-apposed astrocytes (Fig. 9E3) may be the result of the weak intercellular adhesion properties of AQP4[32,41,62]. Moreover, this close association of astrocyte gap junctions and AQP4 water channels suggests that the movement of K^+ and water through the astrocyte syncytium is coordinated by close alignment of both ion- and water-conductive elements from cell to cell.

XIII. Disruptions of O:A gap junctions cause myelin swelling and sclerosis

The original drawing of Brophy (2001) (Fig. 3D, above) provided a new model for understanding saltatory conduction. However, it did not attempt to account for subcellular movements of K^+ (or water) after saltatory conduction, describe inter- or intra-cellular pathways for K^+, or indicate a pathway for sequestration of K^+ by astrocyte processes that were, nevertheless, schematically indicated near nodes of Ranvier. Regardless, two additional elements that now appear to be essential for voltage-augmented K^+ siphoning in myelinated axons of the CNS are:

- **a.** autologous gap junctions between successive paranodal loops of myelin (Fig. 10, *green bars*) to transport K^+ and water from layer to layer, and
- **b.** heterologous O:A gap junctions linking the outermost layer of oligodendrocyte myelin to nearby astrocyte processes (Fig. 10, *green/dark blue bars* and *light green/ light blue bars*), as first shown by Waxman and Black[126] (Fig. 2D).

Interestingly, the original images of Waxman and Black[15,126] emphasized that the astrocyte processes at the nodes of Ranvier formed multiple gap junctions with the outermost paranodal loop of myelin (Fig. 2D1, *arrows and arrow head*; Fig. 2D2, *arrowheads*; shown diagrammatically in Fig. 10). The abundance of these heterologous paranodal gap junctions[45] is presumed to indicate a substantial role for them in normal myelin physiology. More recently, strong evidence that oligodendrocyte gap junctions, including O:A gap junctions, are essential elements for maintaining saltatory conduction, K^+ siphoning, and osmotic homeostasis in myelinated axons of the CNS and PNS has come from studies of several neurologic diseases of human connexins and from genetic knockout (KO) studies of oligodendrocyte and Schwann cell connexins in mice:

A. X-linked Charcot-Marie-Tooth disease (CMTX)

Mutations of the gene on the X-chromosome encoding for Cx32 produce a large group of human genetic diseases collectively called X-linked Charcot-Marie-Tooth disease (CMTX). Symptoms of CMTX include decreased or absent saltatory conduction in the PNS, as well as segmental demyelination[13,110]. Because Cx32 is the primary or sole connexin in gap junctions

between myelin layers in the PNS[9,21,64,109], it was not surprising that the inner and occasionally outer layers of PNS myelin were swollen and separated (Fig. 11A; from112). Those alterations are consistent with influx of K^+ and accompanying osmotic water into innermost adaxonal myelin during sustained or high-frequency axonal saltatory conduction, but in the absence of Cx32-gap junctions in CMTX, that K^+ and water would no longer be able to flow from inner to outer myelin layers via those junctions. The resulting osmotic swelling of cytoplasmic myelin presumably occurs because, in the absence of trans-lamellar gap junctions, K^+ and H_2O must follow the 100-fold to 1000-fold longer spiral pathway around successive paranodal loops[9]. This reduced radial transport and local buildup of K^+ and water, in turn, presumably causes the observed swelling of myelin, and ultimately, segmental demyelination.

Despite altered saltatory conduction of PNS axons in CMTX, there are only limited CNS symptoms[8]. This was an important clue in understanding K^+ siphoning because in the CNS, oligodendrocyte Cx47 may be able to partially compensate for loss of oligodendrocyte Cx32, particularly at O:A gap junctions, which normally contain both connexins[8]. In contrast, there is no potential to compensate for lost or damaged Cx32 in PNS myelin because Schwann cell myelin segments are not coupled by gap junctions to astrocytes or to any other cell. Consequently, long-distance potassium siphoning does not occur in the PNS. Thus, in CMTX, failure to transport K^+ and water between paranodal loops, and radially, through Schmidt-Lanterman incisures, results in osmotic disruption of successive layers of PNS myelin, thereby potentially accounting for the observed high incidence of conduction block in the PNS *vs.* only limited neurologic symptoms in the CNS.

B. Pelizaeus-Merzbacher-like diseases (PMLDs) are a group of debilitating human diseases affecting formation, structure, and function of CNS myelin ("hypomyelination"), with primary symptoms involving reduced conduction velocity and demyelination of long white matter tracts. These "leukodystrophies" (leuko = white [matter]) are now attributed to the mutation or functional knockout of the gene for Cx47[121]. Hereditary spastic paraplegia (HSP) is a second group of diseases with recessive mutation of Cx4787 that results in myelin disruption and consequent altered or blocked axonal saltatory conduction. Because there are no published ultrastructural images of CNS myelin from PMLD or HSP patients, understanding these maladies required examination of tissues from animal models (*i.e.*, mice) having single-knockout for Cx47 and double-knockout for Cx47/Cx32.

C. Cx32/Cx47 double knockout (dKO) mice

In mice, single knockout for Cx32 is not fatal, and an altered phenotype is difficult to detect upon gross physical examination. In contrast, single KO for Cx47 is usually fatal within 100 days of birth due to gross myelin destruction. More debilitating still is the dKO for Cx32 and Cx47, which is always fatal by postnatal day 31 (**P31)**, with severe symptoms and deaths seen as early as P5[66]. In a compelling series of experiments capitalizing on the abrupt increase in activity of the mouse optic nerve following eye opening at P11, Menichella et al.[66] showed by histological examination of Cx32/Cx47 dKO axons (Fig. 11B) that vacuolation of myelin became evident at about P13 (full eye opening and onset of large-scale activity of the myelinated axons of the optic nerve) and became increasingly severe by P15 (Fig. 11B, *top panel, far right*), the age when cage exploration is initiated. Ultrastructural examination of myelinated fibers from P15 optic nerve from the dKO mice revealed that myelin was grossly expanded, particularly in innermost myelin (Fig. 11C, left side), which is the layer most intimately associated with the axolemmal sites of K^+ efflux. However, myelin vacuolation was not detected in age-matched wildtype mice (Fig. 11B, *lower panel*), further suggesting that the onset of vacuolation in the dKO mice was the result of increased and prolonged axonal activity at P15, but without the osmotic protection provided by oligodendrocyte Cx32 and Cx47.

To determine whether the large increase in optic nerve activity in P11-P13 dKO mice was responsible for concurrent development of myelin "vacuoles" or was due to a defect in myelin formation (which also begins at about the same time), Menichella et al. (2006) reduced or eliminated axonal saltatory conduction (Na^+ influx and K^+ efflux) by injecting tetrodotoxin (**TTX**) into the vitreous humor adjacent to the retinas of both normal and Cx32/Cx47 dKO mice (Fig. 11D). This procedure blocked neuronal action potential propagation in retinal ganglion cells, the neurons that form the visual axons within the optic nerve. However, the axons of the optic nerve were not directly exposed to TTX. With all neuronal action potentials arising in the dKO retina blocked by TTX, vacuolization of myelin (Fig. 11D, left side) was greatly reduced or eliminated (Fig. 11D, *right side*). This is consistent with TTX-blockade of Na^+ influx that otherwise would occur during normal saltatory conduction, and as a direct consequence, a concomitant reduction of the efflux of K^+ and H_2O into the peri-internodal compartment. This observation suggests that therapeutic reduction of Na^+ influx (*e.g.*, via "use-dependent" local anesthetics, such as lidocaine111) and attendant reduction of K^+ and H_2O efflux into the peri-internodal space might prove to be an important adjunctive therapy in NMO and several other demyelinating diseases, as proposed in **Section XVII**.

In rapidly-firing axons of dKO animals, the formation of large vacuoles (cytoplasmic edema) primarily in inner myelin is consistent with the hypothesis that blocking gap junction transport pathways between successive myelin layers (via knockout of Cx32-containing gap junctions) prevents radial transport of K^+ and H_2O from inner to outer myelin layers, resulting in swelling of innermost myelin layers. Likewise, deletion of the exit pathway from myelin to astrocytes (via Cx32+Cx47 double KO at O:A gap junctions) prevents transport of K^+ and H_2O into the astrocyte syncytium, leading to gross swelling of outermost myelin, presumably resulting from prolonged back-up of K^+ and accompanying osmotic water into successive cytoplasmic layers of myelin. Because myelin is completely uncoupled from astrocytes in the Cx32/Cx47 dKO mice, and hence, also cannot receive water or K^+ from the astrocytes, the ions and water for swelling of innermost myelin during high-frequency saltatory conduction must be derived from local sources, possibly from the internodal extracellular space and/or the axon cytoplasm (see **Section XVI)**.

XIV. Kir4.1 knockout in astrocytes causes myelin swelling and sclerosis

As part of the study of the role of oligodendrocyte connexins in K^+ siphoning, Menichella, Paul, and co-workers investigated whether disruption of K^+ exit pathways from astrocytes would also cause myelin swelling and vacuolation[66]. Using a Kir4.1 KO mouse (which therefore has greatly reduced K^+ efflux at astrocyte endfeet in optic nerve), they showed that both innermost and outermost myelin layers were osmotically swollen (Figs. 12A1-A2), even though glial gap junctions and astrocyte AQP4 water exit pathways presumably remained intact. Thus, these experiments also showed that disruption of Kir4.1 K^+ exit pathways, alone, was sufficient to cause myelin swelling and necrosis. Moreover, these images were similar to those obtained in the Cx32/Cx47 dKO mouse. These combined data suggested that any substantial disruption in the K^+/H_2O transport pathway, from innermost myelin to the astrocyte endfeet, will ultimately cause ultrastructural alterations of myelin and as a direct consequence, disrupt axonal saltatory conduction.

XV. "Conditional" dKO of astrocyte Cx43/Cx30 causes myelin swelling and sclerosis

Although genetic dKO of Cx43 and Cx30 is embryonic lethal, apparently due to defects in heart development and cardiac electrical activity, as well as to a multitude of other developmental defects[75], conditional double-knockout (**cdKO)** of Cx43 and Cx30 only in astrocytes is not embryonic lethal. Instead, Cx43/Cx30 cdKO results in failure to form gap

junctions between astrocytes and between astrocytes and oligodendrocytes. Notably, these cdKO animals had greatly reduced saltatory conduction[124] and large-scale disruptions of myelin (Fig. 12B), virtually indistinguishable to that seen in Kir4.1 mutants (Fig. 12A) and in Cx32/Cx47 dKO mice (Fig. 10C), and closely resembling that seen in CMTX and PMLD (**Section XIII**). Thus, a common feature of genetic diseases that disrupt myelin and that secondarily interfere with saltatory conduction are defects in the panglial syncytium that interfere with potassium siphoning or associated co- transport of water, as detailed in **Section XVI**.

XVI. Generalized model for potassium siphoning in myelinated axons of CNS

A. Voltage-augmented “dynamic potassium siphoning”

We have proposed a 10-component model for voltage-augmented dynamic potassium siphoning at myelinated axons in the mammalian CNS[45] (Fig. 13):

1. Voltage-gated Nav1 channels localized to the nodal plasma membrane spatially localize inward Na^+ current to the node of Ranvier (*#1* in the diagram).
2. Voltage-gated Kv1 channels (*#2*), restricted to the juxtaparanodal axonal membrane, provide for outward K^+ current across the juxtaparanodal and internodal plasma membrane, into a “privileged” internodal compartment (the “peri-internodal space”) that is not yet clearly defined.
3. K^+ and water enter the innermost cytoplasmic layer of myelin (*#3*), possibly via unidentified K^+ leak channels[94] and as-yet-unidentified aquaporin water channels[5].

   Alternatively, and under conditions of multiple action potentials producing both strong polarization of the peri-internodal compartment and high $[K^+]_P$, the direct structural linkage of gated axonal Kv1 channels with oligodendrocyte Cx29 might allow both K^+ and water to flow directly from the axon cytoplasm into the innermost layer of oligodendrocyte cytoplasm, without efflux into the peri-internodal space, potentially eliminating the need for separate K^+ channels in innermost myelin (but see94). In this model, Kv1 channels linked to Cx29 would be functionally equivalent to and structurally similar to gated connexon channels.
4. Paranode-to-axon septate junctions (*#4*) provide strong diffusion barriers separating the peri-axonal internodal extracellular space from the extracellular space at each node of Ranvier. These strong diffusion barriers help to maintain the transient high $[K^+]$ in the peri-internodal compartment. This high potassium concentration in the peri-internodal compartment would create a voltage difference across the paranodal loops of myelin that would effectively drive K^+ from the positive voltage of the peri-internodal space/innermost paranodal loop (+75 mV), through successive layers of paranodal myelin, to the negative membrane potential of astrocyte endfeet (−85 mV) – a potential difference (driving force) of +160 mV.
5. Cx32-gap junctions link cytoplasmic myelin lamellae at successive paranodal loops[55] (*#5*), shortening the radial pathway by 100- to 1000-fold[9] and facilitating voltage-augmented transport of K^+ between myelin layers. These gap junctions may also create a mechanism for regulating voltage steps between successive paranodal loops137. Structurally and diagrammatically, the stacks of paranodal myelin, linked by gap junctions and having a voltage gradient from peri-internodal compartment to outermost myelin, closely resemble a Cockroft-Walton voltage multiplier assembly25،116. This configuration of membranes linked by gap junctions may also provide a mechanism for voltage-accumulation, voltage-stepping, and voltage-shunting that may be integral to saltatory nerve conduction at prolonged high

stimulation frequencies. Voltage shunting and current flow through the interlamellar gap junctions might then be temporally modulated (via Cx32 channel gating137) to further facilitate saltatory conduction at different stimulation frequencies.

6. O:A gap junctions (*#6*) allow intercellular fluxes of K^+ and water into the astrocyte syncytium, thereby rapidly equilibrating $[K^+]_I$ from successive myelin segments into different astrocyte compartments.

7. A:A gap junctions (*#7*) and their closely associated AQP4 arrays facilitate efficient voltage-augmented transport of K^+ and H_2O throughout the much larger tissue volume of the broader astrocyte syncytium[22].

8. Efflux of K^+ from astrocytes occurs at Kir4.1 K^+ channels (*#8*) that are concentrated in astrocyte endfeet.

9. Efflux and co-transport of osmotic water occurs via abundant AQP4 water channels (*#9*) at the same astrocyte endfeet.

10. Axonal K^+ and associated osmotic water (which were lost during saltatory conduction and transported to and released at astrocyte endfeet) must be replaced from the extracellular space, either at the nodes of Ranvier (*#10*) or at neuronal somata and dendrites.

A similar model for roles of gap junctions, Kir4.1 and AQP4 in potassium siphoning was subsequently proposed by Menichella and coworkers[66].

B. Electrical and osmotic driving forces for K^+ and water during K^+ siphoning

1. Based on measurements made by David and coworkers, there appears to be a −90 mV to −160 mV driving force on positively-charged K^+, from the peri-internodal compartment (+5 mV to +75 mV)28,29 to the astrocyte endfeet (−85 mV) (Fig. 13). This electrical voltage gradient (electrical driving force) would greatly augment the ion fluxes over that attributable to passive K^+ spatial buffering. Moreover, this proposed variable voltage gradient across the paranodal loops of myelin might also serve to gate Cx29 hemichannels in the adaxonal myelin plasma membrane, allowing axonal K^+ directly into the innermost cytoplasmic layer of myelin.

2. There is also a strong osmotic driving force on K^+ (*i.e.*, 20-100 mM in the peri-internodal compartment *vs.* 2-3 mM in the extracellular space around astrocyte endfeet) that would greatly facilitate movement of K^+ toward areas of low $[K^+]_O$ at astrocyte endfeet. And as K^+ moves, so must the accompanying intracellular osmotic water, possibly augmented by their interaction with negatively-charged glial fibrillary acidic protein (GFAP) filaments that permeate virtually the entire astrocyte syncytium[22].

These two strong driving forces would result in voltage-augmented potassium siphoning and osmotic co-transport of water, from innermost myelin, through the panglial syncytium, to release at astrocyte endfeet that surround capillaries and that form the glia limitans. Thus, this proposal extends the original concept of passive “potassium spatial buffering” or “potassium siphoning” near unmyelinated axons to a process of voltage-augmented “dynamic” potassium siphoning in myelinated axons of higher vertebrates. New experimental approaches will be required to more fully investigate this hypothesis.

XVII. Autoimmune destruction of AQP4 in astrocyte endfeet *vs.* large-scale oligodendrocyte demyelination and sclerosis in NMO

A. Historical and current diagnosis of NMO

Neuromyelitis optica [38; also called Devic's disease30], an especially aggressive form of multiple sclerosis (**MS**), was originally defined as an idiopathic, severe demyelinating disease that is restricted to CNS myelin but that does not affect PNS myelin (*i.e.*, affects oligodendrocytes but not Schwann cells). NMO preferentially affects myelin of the optic nerves (optic neuritis) and spinal cord (transverse myelitis), both of which contain long-distance, frequently- or constantly-activated myelinated axons. Non-Caucasians (Asians and Africans) are affected preferentially, with women affected *ca.* 9 times as frequently as men (average age of onset *ca.* 39), apparently reflecting the more robust immune systems created by expression of two X-chromosomes in women. NMO is also an inflammatory CNS disease in children[63], with equally debilitating effects. Although symptoms of NMO closely resemble those of conventional MS, NMO was differentiated from MS by: *a)* its distinctive optic and spinal cord symptoms and *b)* the size of its sclerotic plaques (spanning three or more contiguous vertebral segments)[53,130].

Before 2000, the prognosis for NMO patients was that 20% would be blind in one or both eyes, require ambulatory support, or die within five years, usually from respiratory failure due to demyelination/sclerosis of descending motor tracts in the spinal cord. At that time, there were no definitive diagnostic tests to distinguish between conventional MS and NMO. However, NMO was recently demonstrated to be a primary autoimmune disease directed against AQP4 water channels[130], which in the CNS are concentrated primarily in astrocyte endfeet[72,83,107]. This posed a problem in understanding the etiology of NMO because, with the exception of the diminished blood-brain barrier at the circumventricular organs and at the entry point of axons into the optic nerve in the retina, most areas of high AQP4 expression in the brain are within and normally protected by the blood-brain barrier. However, new diagnostic tests, based on detection of AQP4 antibodies[53], combined with MRI detection of large sclerotic plaques in optic nerve and spinal cord, have allowed unambiguous diagnosis of NMO *vs.* other forms of MS. With these improved diagnostic criteria, NMO is now recognized to represent *ca.* 10% of cases formerly thought to be MS, corresponding to a remarkable >70 cases per month diagnosed by referral to Mayo Clinic in 2008 (Dr. Vanda Lennon, personal communication). Despite this progress, the AQP4-mediated, astrocyte-directed immunological basis for inflammatory swelling and destruction of CNS myelin in NMO remains unexplained, primarily because CNS myelin is formed by oligodendrocytes, which are far removed from the primary immunological target at astrocyte endfeet.

B. A new model for myelin destruction in NMO

Autoimmune destruction of AQP4 water channels in astrocyte endfeet of NMO patients appears to exert its primary neurological effect by disrupting essential water exit pathways that would otherwise dispose of the large volume of intracellular osmotic water that accompanies K^+ into the inner layers of CNS myelin following axonal saltatory conduction. According to this model, if this osmotic load on myelin is not rapidly dispersed by large-scale potassium siphoning, osmotically-associated water builds up in cytoplasmic myelin (paranodes and innermost and outermost myelin), which then expand and ultimately burst, similar to that demonstrated following double knockout of Cx32+Cx47[66] (Fig. 11C) and Cx43+Cx30[59] (Fig. 12B), as well as following single KO of Kir4.1[66] (Fig. 12A). Accordingly, disruptions of myelin are particularly pronounced in the highly-active optic nerve, as well as in the axons of the constantly-activated descending respiratory motor tracts of the spinal cord. However, according to this model, damage to myelin would be predicted in other active white matter tracts, including the corpus callosum and other axon bundles that lie adjacent to

circumventricular organs, where the blood brain barrier is absent, a prediction that was recently confirmed[92,138]. These pathological disruptions of water exit pathways in NMO lead to osmotic swelling of paranodal loops and of innermost and outermost cytoplasmic layers of myelin, resulting in overall myelin swelling, oligodendrocyte necrosis, and ultimately to formation of sclerotic plaques over progressively larger areas as the water exit pathways are progressively destroyed, axons are induced to increase firing to compensate for reduced saltatory conduction, and the osmotic burden on remaining myelin segments rises precipitously.

C. Potential new avenues for treatment of patients with NMO

The model for dynamic potassium siphoning via the panglial syncytium predicts that normal homeostatic repair mechanisms are progressively overwhelmed as more and more astrocytes and oligodendrocytes are damaged or destroyed. However, before necrosis of the majority of oligodendrocytes occurs, the initial destructive changes (*i.e.*, swelling of paranodal loops and of cytoplasmic myelin) might be partially reversed based on therapies that reduce Na^+ influx, and hence reduce K^+ efflux during normal saltatory conduction. With a large "safety factor" of Na^+ influx and K^+ efflux during each action potential, administration of "use-dependent" local anesthetics (*e.g.*, lidocaine) and of "K^+-sparing" drugs (*e.g.*, Tegretol/carbamazepine) may reduce the ionic/osmotic load on individual myelin segments, as well as collectively on major expanses of the panglial syncytium. In combination with plasmapheresis and immunosuppressive therapy to reduce ongoing autoimmune damage to astrocyte endfeet, "K^+ sparing" therapies may further reduce cellular damage to myelin, and allow ongoing homeostatic cellular repair mechanisms in those few surviving oligodendrocytes to remyelinate damaged axons. Finally, after the autoimmune destructive process is controlled, newly-developed stem cell therapies using oligodendrocyte precursor cells[132] may be able to induce re-myelination of large expanses of demyelinated axons, thereby partially restoring normal function in patients with this otherwise debilitating or fatal autoimmune disease.

Acknowledgments

Dr. Rash's research described in this review was supported in part by grants from the NIH (NS44395, NS31027, NS44010, NS38121, NS39040, S10RR08329, S10RR05831), grants from NIH to Peter Agre (HL33991, HL48268, EY11239) and the Human Frontier Science Program, grants to Soren Nielsen (Karen Elise Jensen Foundation and the Novo Nordisk Foundation), grants to Edward Dudek (NIH MH55595 and NS16683) and UA Air Force Office of Scientific Research, and grants to James I. Nagy (CIHR and the Medical Research Council of Canada).

I wish to thank Ms. Kimberly G. V. Davidson for redrawing Fig. 3D and for original artwork as Figs. 5, 10, and 13. I also thank Ms. Davidson, Mr. Thomas Yasumura, and Dr. Sue Furman for making and examining FRIL samples and for careful reading of the manuscript, and Drs. Vanda Lennon, Naomi Kamasawa, and Sue Furman for critical discussions and comments on early versions of the manuscript.

Reference List

1. Ahn M, Lee J, Gustafsson A, Enriquez A, Lancaster E, Sul J-Y, Haydon PG, Paul DL, Huang Y, Abrams CK, Scherer S. Cx29 and Cx32, two connexins expressed by myelinating glia, do not interact and are functionally distinct. J Neurosci Res 2008;86:992–1006. [PubMed: 17972320]
2. Akiyama Y, Radtke C, Kocsis JD. Remyelination of the rat spinal cord by transplantation of identified bone marrow stromal cells. J Neurosci 2002;22:6623–6630. [PubMed: 12151541]
3. Altevogt BM, Kleopas KA, Postma FR, Scherer SS, Paul D. Connexin29 is uniquely distributed within myelinating glial cells of the central and peripheral nervous systems. J Neurosci 2002;22:6458–6470. [PubMed: 12151525]
4. Altevogt BM, Paul DL. Four classes of intercellular channels between glial cells in the CNS. J Neurosci 2004;24:4313–4323. [PubMed: 15128845]
5. Amiry-Moghaddam M, Ottersen OP. The molecular basis of water transport in the brain. Nature Reviews: Neuroscience 2003;4:991–1002.

6. Arroyo EJ, Scherer SS. On the molecular architecture of myelinated fibers. Histochem Cell Biol 2000;113:1–18. [PubMed: 10664064]
7. Arroyo EJ, Sirkowski EE, Chitale R, Scherer SS. Acute demyelination disrupts the molecular organization of peripheral nervous system nodes. J Comp Neurol 2004;479:424–434. [PubMed: 15514980]
8. Bahr M, Andres F, Timmerman V, Nelis ME, Van Broeckhoven C, Dichgans J. Central visual, acoustic, and motor pathway involvement in a Charcot-Marie-Tooth family with an Asn205Ser mutation in the connexin 32 gene. J Neurol Neurosurg Psychiatry 1999;66:202–206. [PubMed: 10071100]
9. Balice-Gordon RJ, Bone LJ, Scherer SS. Functional gap junctions in the Schwann cell myelin sheath. J Cell Biol 1998;142:1095–1104. [PubMed: 9722620]
10. Baranova A, Ivanov D, Petrash N, Pestova A, Skoblov M, Kelmanson I, Shagin D, Nazarenko S, Geraymovych E, Litvin O. The mammalian pannexin family is homologous to the invertebrate innexin gap junction proteins. Genomics 2004;83:706–716. [PubMed: 15028292]
11. Barbe MT, Monyer H, Bruzzone R. Cell-cell communication beyond connexins: The pannexin channels. Physiology 2006;21:103–114. [PubMed: 16565476]
12. Baumgartner S, Littleton JT, Broadie K, Bhat MA, Harbecke R, Lengyel JA, Chiquet-Ehrismann R, Prokop A, Bellen HJ. A Drosophila neurexin is required for septate junction and blood-nerve barrier formation and function. Cell 1996;87:1059–1068. [PubMed: 8978610]
13. Bergoffen J, Scherer SS, Wang S, Oronzi-Scott M, Paul D, Chen K, Lensch MW, Chance P, Fischbeck K. Connexin mutations in X-linked Charcot-Marie-Tooth disease. Science 1993;262:2039–2042. [PubMed: 8266101]
14. Bhat MA, Rios JC, Lu Y, Garcia-Fresco GP, Ching W, Martin MS, Li J, Einheber S, Chesler M, Rosenbluth J, Salzer JL, Bellen HJ. Axon-glia interactions and the domain organization of myelinated axons requires neurexin IV/caspr/paranodin. Neuron 2001;30:369–383. [PubMed: 11395000]
15. Black JA, Waxman SG. The perinodal astrocyte. Glia 1988;1:169–183. [PubMed: 2976037]
16. Boyle MET, Berglund EO, Murai KK, Weber L, Peles E, Ranscht B. Contactin orchestrates assembly of the septate-like junctions at the paranode in myelinated peripheral nerve. Neuron 2001;30:385–397. [PubMed: 11395001]
17. Brightman MW, Reese TS. Junctions between intimately apposed cell membranes in the vertebrate brain. J Cell Biol 1969;40:648–677. [PubMed: 5765759]
18. Brophy PJ. Axoglial junctions: Separate the channels or scramble the message. Current Biology 2001;11:R555–R557. [PubMed: 11509252]
19. Brophy PJ. Myelinated nerves: Filling in the juxtaparanodal gap. Curr Biol 2003;13:R956–R957. [PubMed: 14680652]
20. Bruzzone R, Hormuzdi SG, Barbe MT, Herb A, Monyer H. Pannexins, a family of gap junction proteins expressed in brain. Proc Natl Acad Sci (USA) 2003;100:13644–13649. [PubMed: 14597722]
21. Bruzzone R, White TW, Paul DL. Connections with connexins: the molecular basis of direct intercellular signaling. Europ J Biochem 1996;238:1–27. [PubMed: 8665925]
22. Bushong EA, Martone ME, Jones YZ, Ellisman MH. Protoplasmic astrocytes in CA1 stratum radiatum occupy separate anatomical domains. J Neurosci 2002;22:183–192. [PubMed: 11756501]
23. Butt AM, Ransom BR. Visualization of oligodendrocytes and astrocytes in the intact rat optic nerve by intracellular injection of Lucifer Yellow and horseradish peroxidase. Glia 1989;2:470–475. [PubMed: 2531727]
24. Chiu SY, Ritchie JM. Potassium channels in nodal and internodal axonal membrane of mammalian myelinated fibres. Nature 1980;284:170–171. [PubMed: 6244497]
25. Cockcroft JD, Walton ETS. Experiments with high velocity positive ions. II The disintegration of elements by high velocity protons. Proc R Soc London, Ser A 1932;137:229–242.
26. Coppen SR, Kaba RA, Halliday D, Dupont E, Skepper JN, Elneil S, Severs NJ. Comparison of connexin expression patterns in the developing mouse heart and human foetal heart. Mol Cell Biochem 2003;242:121–127. [PubMed: 12619874]
27. Crane JM, Verkman AS. Determinants of aquaporin-4 assembly in orthogonal arrays revealed by live-cell single-molecule fluorescence imaging. J Cell Sci 2009;122:813–821. [PubMed: 19240114]

28. David G, Barrett JN, Barrett EF. Evidence that action potentials activate an internodal potassium conductance in lizard myelinated axons. J Physiol 1992;445:277–301. [PubMed: 1501136]
29. David G, Barrett JN, Barrett EF. Activation of internodal potassium conductance in rat myelinated axons. J Physiol 1993;472:177–202. [PubMed: 8145140]
30. Devic E. Myélite subaiguë compliquée de névrite optique. Bull Med (Paris) 1894;8:1033–1034.
31. Einheber S, Zanazzi G, Ching W, Scherer S, Milner TA, Peles E, Salzer JL. The axonal membrane protein Caspr, a homologue of neurexin IV, is a component of the septate-like paranodal junctions that assemble during myelination. J Cell Biol 1997;139:1495–1506. [PubMed: 9396755]
32. Engel A, Fujiyoshi Y, Gonen T, Walz T. Junction-forming aquaporins. Curr Opinion Struc Biol 2008;18:229–235.
33. Evans WH, Martin PEM. Gap junctions: structure and function. Mol Membr Biol 2002;19:121–136. [PubMed: 12126230]
34. Filippov MA, Hormuzdi SJ, Fuchs EC, Monyer H. A reporter allele for investigating connexin 26 gene expression in the mouse brain. Eur J Neurosci 2003;18:3183–3192. [PubMed: 14686892]
35. Fujimoto K. Freeze-fracture replica electron microscopy combined with SDS digestion for cytochemical labeling of integral membrane proteins. Application to the immunogold labeling of intercellular junctional complexes. J Cell Sci 1995;108:3443–3449. [PubMed: 8586656]
36. Fujimoto K. SDS-digested freeze-fracture replica labeling electron microscopy to study the two-dimensional distribution of integral membrane proteins and phospholipids in biomembranes: practical procedure, interpretation and application. Histochem Cell Biol 1997;107:87–96. [PubMed: 9062793]
37. Furman CS, Gorelick-Feldman DA, Davidson KGV, Yasumura T, Neely JD, Agre P, Rash JE. Aquaporin-4 square array assembly: Opposing actions of M1 and M23 isoforms. Proc Natl Acad Sci (USA) 2003;100:13609–13614. [PubMed: 14597700]
38. Gault, F. De la neuromyélite optique aiguë. Lyon, France: Lyon University; 1894.
39. Goldstein SAN, Bockenhauer D, O'Kelly I, Zilberberg N. Potassium leak channels and the KCNK family of two-p-domain subunits. Nat Rev Neurosci 2001;2:175–184. [PubMed: 11256078]
40. Hille, B. Ionic Channels of Excitable Membranes. Sinauer Associates, Inc; Sunderland, MA: 1992. p. 1-607.
41. Hiroaki Y, Tani K, Kamegawa A, Gyobu N, Nishikawa K, Suzuki H, Walz T, Sasaki S, Mitsuoka K, Kimura K, Mizoguchi A, Fujiyoshi Y. Implications of the aquaporin-4 structure on array formation and cell adhesion. J Mol Biol 2006;355:628–639. [PubMed: 16325200]
42. Hodgkin AL. The ionic basis of electrical activity in nerve and muscle. Biol Rev 1951;26:339–409.
43. Hodgkin AL, Huxley AF. A quantitative description of membrane current and its application to conduction and excitation in nerve. J Physiol 1952;117:500–544. [PubMed: 12991237]
44. Hu X, Dahl G. Exchange of conductance and gating properties between gap junction hemichannels. FEBS Letters 1999;451:113–117. [PubMed: 10371149]
45. Kamasawa N, Sik A, Morita M, Yasumura T, Davidson KGV, Nagy JI, Rash JE. Connexin47 and connexin32 in gap junctions of oligodendrocyte somata, myelin sheaths, paranodal loops, and Schmidt-Lanterman incisures: Implications for ionic homeostasis and potassium siphoning. Neuroscience 2005;136:65–86. [PubMed: 16203097]
46. Kettenmann H, Ransom BR. Electrical coupling between astrocytes and between oligodendrocytes studied in mammalian cell cultures. Glia 1988;1:64–73. [PubMed: 2853139]
47. Kleopa KA, Orthmann JL, Enriquez A, Paul DL, Scherer SS. Unique distributions of the gap junction proteins connexin29, connexin32, and connexin47 in oligodendrocytes. Glia 2004;47:346–357. [PubMed: 15293232]
48. Kofuji P, Newman EA. Potassium buffering in the central nervous system. Neuroscience 2004;129:1043–1054.
49. Kunzelmann P, Schroder W, Traub O, Steinhauser C, Dermietzel R, Willecke K. Late onset and increasing expression of the gap junction protein connexin30 in adult murine brain and long-term cultured astrocytes. Glia 1999;25:111–119. [PubMed: 9890626]
50. Landis DMD. Membrane structure in mammalian astrocytes: A review of freeze-fracture studies on adult, developing, reactive and cultured astrocytes. J Exp Biol (Brit) 1981;95:35–48.

51. Landis DMD, Reese TS. Arrays of particles in freeze-fractured astrocytic membranes. J Cell Biol 1974;60:316–320. [PubMed: 4809245]
52. Larsen WJ. Biological implications of gap junction structure, distribution and composition: A review. Tissue and Cell 1983;15:645–671. [PubMed: 6359583]
53. Lennon VA, Wingerchuk DM, Kryzer TJ, Pittock SJ, Lucchinetti CF, Fujihara K, Nakashima I, Weinshenker BG. A serum autoantibody marker of neuromyelitis optica: distinction from multiple sclerosis. Lancet 2004;364:2106–2112. [PubMed: 15589308]
54. Li J, Hertzberg EL, Nagy JI. Connexin32 in oligodendrocytes and association with myelinated fibers in mouse and rat brain. J Comp Neurol 1997;379:571–591. [PubMed: 9067844]
55. Li X, Ionescu A-V, Lynn BD, Lu S, Kamasawa N, Morita M, Davidson KGV, Yasumura T, Rash JE, Nagy JI. Connexin47, connexin29 and connexin32 co-expression in oligodendrocytes and Cx47 association with zonula occludens-1 (ZO-1) in mouse brain. Neuroscience 2004;126:611–630. [PubMed: 15183511]
56. Li X, Kamasawa N, Ciolofan C, Olson CO, Lu S, Davidson KGV, Yasumura T, Shigemoto R, Rash JE, Nagy JI. Connexin45-containing neuronal gap junctions in rodent retina also contain connexin36 in both apposing hemiplaques, forming bi-homotypic gap junctions, with scaffolding contributed by zonula occludens-1. J Neurosci 2008;28:9769–9789. [PubMed: 18815262]
57. Li X, Lynn BD, Olson C, Meier C, Davidson KGV, Yasumura T, Rash JE, Nagy JI. Connexin29 expression, immunocytochemistry and freeze-fracture replica immunogold labeling (FRIL) in sciatic nerve. Eur J Neurosci 2002;16:795–806. [PubMed: 12372015]
58. Loewenstein WR. Permeability of membrane junctions. Ann N Y Acad Sci 1966:441–472. [PubMed: 5229810]
59. Lutz SE, Zhao Y, Gulinello M, Lee SC, Raine CS, Brosnan CF. Deletion of astrocyte connexins 43 and 30 leads to a dysmyelinating phenotype and hippocampal CA1 vacuolation. J Neuroscience 2009;29:7743–7752.
60. Massa PT, Mugnaini E. Cell junctions and intramembrane particles of astrocytes and oligodendrocytes: a freeze-fracture study. Neuroscience 1982;7:523–538. [PubMed: 7078735]
61. Matthews MA, Duncan D. A quantitative study of morphological changes accompanying the initiation and progress of myelin production in the dorsal funiculus of the rat spinal cord. J Comp Neurol 1971;142:1–22. [PubMed: 4103051]
62. McCoy E, Sontheimer H. Expression and function of water channels (aquaporins) in migrating malignant astrocytes. Glia 2007;55:1034–1043. [PubMed: 17549682]
63. McKeon A, Lennon VA, Lotze T, Tenenbaum S, Ness JM, Rensel M, Kuntz NL, Fryer JP, Homburger H, Weinshenker BG, Krecke K, Lucchinetti CF, Pittock SJ. CNS aquaporin-4 autoimmunity in children. Neurology 2008;71:93–100. [PubMed: 18509092]
64. Meier C, Dermietzel R, Davidson KGV, Yasumura T, Rash JE. Connexin32-containing gap junctions in Schwann cells at the internodal zone of partial myelin compaction and in Schmidt-Lanterman incisures. J Neurosci 2004;24:3186–3198. [PubMed: 15056698]
65. Menichella DM, Goodenough DA, Sirkowski E, Scherer SS, Paul DL. Connexins are critical for normal myelination in the CNS. J Neurosci 2003;23:5963–5973. [PubMed: 12843301]
66. Menichella DM, Majdan M, Awatramani R, Goodenough DA, Sirkowski E, Scherer SS, Paul DL. Genetic and physiological evidence that oligodendrocyte gap junctions contribute to spatial buffering of potassium released during neuronal activity. J Neurosci 2006;26:10984–10991. [PubMed: 17065440]
67. Miller RG, Pinto da Silva P. Particle rosettes in the periaxonal Schwann cell membrane and particle clusters in the axolemma of rat sciatic nerve. Brain Res 1977;130:135–141. [PubMed: 884515]
68. Moe SE, Sorbo JG, Sogaard R, Zeuthen T, Petter Ottersen O, Holen T. New isoforms of rat Aquaporin-4. Genomics 2008;91:367–377. [PubMed: 18255256]
69. Mugnaini, E. Cell junctions of astrocytes, ependyma, and related cells in the mammalian central nervous system, with emphasis on the hypothesis of a generalized functional syncytium of supporting cells. In: Fedoroff, S.; Vernadakis, A., editors. Astrocytes. Vol. I. Academic Press; New York: 1986. p. 329-371.
70. Nagelhus EA, Horio Y, Inanobe A, Fujita A, Haug F-M, Nielsen S, Kurachi Y, Ottersen OP. Immunogold evidence suggests that coupling of K^+ siphoning and water transport in rat retinal Muller

cells is mediated by coenrichment of Kir4.1 and AQP4 in specific membrane domains. Glia 1999;26:47–54. [PubMed: 10088671]

71. Nagelhus EA, Mathiisen TM, Ottersen OP. Aquaporin-4 in the central nervous system: Cellular and subcellular distribution and coexpression with KIR4.1. Neuroscience 2004;129:905–913. [PubMed: 15561407]
72. Nagelhus EA, Veruki ML, Torp R, Haug F-M, Laake JH, Nielsen S, Agre P, Ottersen OP. Aquaporin-4 water channel protein in the rat retina and optic nerve: Polarized expression of Müller cells of fibrous astrocytes. J Neurosci 1998;18:2506–2519. [PubMed: 9502811]
73. Nagy JI, Dudek FE, Rash JE. Update on connexins and gap junctions in neurons and glia in the mammalian central nervous system. Brain Res Brain Res Rev 2004;47:191–215. [PubMed: 15572172]
74. Nagy JI, Ionescu A-V, Lynn BD, Rash JE. Connexin29 and connexin32 at oligodendrocyte and astrocyte gap junctions and in myelin of the mouse central nervous system. J Comp Neurol 2003;464:356–370. [PubMed: 12900929]
75. Nagy JI, Ionescu A-V, Lynn BD, Rash JE. Coupling of astrocyte connexins Cx26, Cx30, Cx43 to oligodendrocyte Cx29, Cx32, Cx47: Implications from normal and connexin32 knockout mice. Glia 2003;44:205–218. [PubMed: 14603462]
76. Nagy JI, Li WEI, Roy C, Doble BW, Gilchrist JS, Kardami E, Hertzberg EL. Selective monoclonal antibody recognition and cellular localization of an unphosphorylated form of connexin43. Exptl Cell Res 1997;236:127–136. [PubMed: 9344592]
77. Nagy JI, Li X, Rempel J, Stelmack GL, Patel D, Staines WA, Yasumura T, Rash JE. Connexin26 in adult rodent CNS: Demonstration at astrocytic gap junctions and co-localization with connexin30 and connexin43. J Comp Neurol 2001;441:302–323. [PubMed: 11745652]
78. Nagy JI, Patel D, Ochalski PAY, Stelmack GL. Connexin30 in rodent, cat and human brain: Selective expression in gray matter astrocytes, co-localization with connexin43 at gap junctions and late developmental appearance. Neuroscience 1990;88:447–468. [PubMed: 10197766]
79. Neely JD, Christensen BM, Nielsen S, Agre P. Heterotetrameric composition of aquaporin-4 water channels. Biochemistry 1999;38:11156–11163. [PubMed: 10460172]
80. Neuhaus J, Schmid E-M, Wolburg H. Stability of orthogonal arrays of particles in murine skeletal muscle and astrocytes after circulator arrest. Neurosci Let 1990;109:163–168. [PubMed: 2314629]
81. Newman EA. High potassium conductance in astrocyte endfeet. Science 1986;233:453–454. [PubMed: 3726539]
82. Newman EA, Frambach DA, Odette LL. Control of extracellular potassium levels by retinal glial cell K+ siphoning. Science 1984;225:1174–1175. [PubMed: 6474173]
83. Nielsen S, Nagelhus EA, Amiry-Moghaddam M, Bourque C, Agre P, Ottersen OP. Specialized membrane domains for water transport in glial cells: High-resolution immunogold cytochemistry of aquaporin-4 in rat brain. J Neurosci 1997;17:171–180. [PubMed: 8987746]
84. Ochalski PAY, Frankenstein UN, Hertzberg EL, Nagy JI. Connexin43 in rat spinal cord: localization in astrocytes and identification of heterotypic astro-oligodendrocytic gap junctions. Neuroscience 1997;76:931–945. [PubMed: 9135062]
85. Orkand RK, Nicholls JG, Kuffler SW. Effect of nerve impulses on the membrane potential of glial cells in the central nervous system of amphibia. J Neurophysiol 1966;29:788–806. [PubMed: 5966435]
86. Orthmann-Murphy JL, Freidin M, Fischer E, Scherer SS, Abrams CK. Two distinct heterotypic channels mediate gap junction coupling between astrocyte and oligodendrocyte connexins. J Neurosci 2007;27:13949–13957. [PubMed: 18094232]
87. Orthmann-Murphy JL, Salsano E, Abrams CK, Bizzi A, Uziel G, Freidin MM, Lamantea E, Zeviani M, Scherer SS, Pareyson D. Hereditary spastic paraplegia is a novel phenotype for GJA12/GJC2 mutations. Brain awn 2009:328.
88. Panchin Y, Kelmanson I, Matz M, Lukyanov K, Usman N, Lukyanov S. A ubiquitous family of putative gap junction molecules. Curr Biol 2000;10:R473–R474. [PubMed: 10898987]
89. Panchin YV. Evolution of gap junction proteins - the pannexin alternative. J Exp Biol 2005;208:1415–1419. [PubMed: 15802665]

90. Pastor A, Kremer M, Möller T, Kettenmann H, Dermietzel R. Dye coupling between spinal cord oligodendrocytes: Differences in coupling efficiency between gray and white matter. Glia 1998;24:108–120. [PubMed: 9700494]

91. Peters, A.; Palay, SL.; Webster, HD. Neurons and Their Supporting Cells. Oxford University Press; New York: 1991. The Fine Structure of the Nervous System; p. 1-494.

92. Pittock SJ, Weinshenker BG, Lucchinetti CF, Wingerchuk DM, Corboy JR, Lennon VA. Neuromyelitis optica brain lesions localized at sites of high aquaporin 4 expression. Arch Neurol 2006;63:964–968. [PubMed: 16831965]

93. Poliak S, Salomon D, Elhanany H, Sabanay H, Kiernan B, Pevny L, Stewart CL, Xu X, Chiu SY, Shrager P, Furley AJW, Peles E. Juxtaparanodal clustering of Shaker-like K+ channels in myelinated axons depends on Caspr2 and TAG-1. J Cell Biol 2003;162:1149–1160. [PubMed: 12963709]

94. Poopalasundaram S, Knott C, Shamotienko OG, Foran PG, Dolly JO, Ghiani CA, Gallo V, Wilkin GP. Glial heterogeneity in expression of the inwardly rectifying K(+) channel, Kir4.1, in adult rat CNS. Glia 2000;30:362–372. [PubMed: 10797616]

95. Purves, D.; Augustine, GJ.; Fitzpatrick, D.; Katz, LC.; LaMantia, A-S.; McNamara, JO.; Williams, SM. Neuroscience. Sinauer Associates, Inc; Sunderland, MA: 2001.

96. Ranvier L-A. Contributions a la histologie et a la physiologie des nerf peripheriques. C R Hebd Seances Acad Sci (Paris) 1871;73:1168–1171.

97. Rasband MN. It's "juxta" potassium channel! J Neurosci Res 2004;76:749–757. [PubMed: 15160387]

98. Rasband MN, Peles E, Trimmer JS, Levinson SR, Lux SE, Shrager P. Dependence of nodal sodium channel clustering on paranodal axoglial contact in the developing CNS. J Neurosci 1999;19:7516–7528. [PubMed: 10460258]

99. Rasband MN, Shrager P. Ion channel sequestration in central nervous system axons. J Physiol (Lond) 2000;525:63–73. [PubMed: 10811725]

100. Rash, JE. The sectioned-replica technique: Direct correlation of freeze-fracture replicas and conventional thin-section images. In: Rash, JE.; Hudson, CS., editors. Freeze-fracture: Methods, artifacts and interpretations. Raven Press; NY: 1979. p. 153-159.

101. Rash, JE.; Dillman, RK.; Morita, M.; Whalen, LR.; Guthrie, PB.; Fay-Guthrie, D.; Wheeler, DW. Grid-mapped freeze fracture: Correlative confocal laser scanning microscopy and freeze-fracture electron microscopy of preselected cells in tissue slices. In: Severs, NJ.; Shotton, DM., editors. Rapid Freezing, Freeze Fracture, and Deep Etching. Wiley-Liss, Inc; New York, NY: 1995. p. 127-150.

102. Rash JE, Duffy HS, Dudek FE, Bilhartz BL, Whalen LR, Yasumura T. Grid-mapped freeze-fracture analysis of gap junctions in gray and white matter of adult rat central nervous system, with evidence for a "panglial syncytium" that is not coupled to neurons. J Comp Neurol 1997;388:265–292. [PubMed: 9368841]

103. Rash JE, Olson CO, Pouliot WA, Davidson KGV, Yasumura T, Furman CS, Royer S, Kamasawa N, Nagy JI, Dudek FE. Connexin36, miniature neuronal gap junctions, and limited electrotonic coupling in rodent suprachiasmatic nucleus. Neuroscience 2007;149:350–371. [PubMed: 17904757]

104. Rash JE, Yasumura T. Direct immunogold labeling of connexins and aquaporin4 in freeze-fracture replicas of liver, brain and spinal cord: factors limiting quantitative analysis. Cell Tissue Res 1999;296:307–321. [PubMed: 10382274]

105. Rash JE, Yasumura T, Davidson K, Furman CS, Dudek FE, Nagy JI. Identification of cells expressing Cx43, Cx30, Cx26, Cx32 and Cx36 in gap junctions of rat brain and spinal cord. Cell Commun Adhes 2001;8:315–320. [PubMed: 12064610]

106. Rash JE, Yasumura T, Dudek FE, Nagy JI. Cell-specific expression of connexins, and evidence for restricted gap junctional coupling between glial cells and between neurons. J Neurosci 2001;21:1983–2001. [PubMed: 11245683]

107. Rash JE, Yasumura T, Hudson CS, Agre P, Nielsen S. Direct immunogold labeling of aquaporin-4 in "square arrays" of astrocyte and ependymocyte plasma membranes in rat brain and spinal cord. Pro Natl Acad Sci 1998;95:11981–11986.

108. Rios JC, Rubin M, St Martin M, Downey RT, Einheber S, Rosenbluth J, Levinson SR, Bhat M, Salzer JL. Paranodal interactions regulate expression of sodium channel subtypes and provide a diffusion barrier for the node of Ranvier. J Neurosci 2003;23:7001–7011. [PubMed: 12904461]

109. Scherer SS, Deschenes SM, Xu Y-T, Grinspan JP, Fischbeck KH, Paul DL. Connexin32 is a myelin-related protein in the PNS and CNS. J Neurosci 1995;15:8281. [PubMed: 8613761]

110. Scherer SS, Xu YT, Nelles E, Fischbeck K, Willecke K, Bone LJ. Connexin32-null mice develop demyelinating peripheral neuropathy. Glia 1998;24:8–20. [PubMed: 9700485]

111. Schwarz W, Palade PT, Hille B. Local anesthetics. Effect of pH on use-dependent block of sodium channels in frog muscle. Biophysical Journal 1977;20:343–368. [PubMed: 21711]

112. Senderek J, Hermanns B, Bergmann C, Boroojerdi B, Bajbouj M, Hungs M, Ramaekers VT, Quasthoff S, Karch D, Schroder JM. X-linked dominant Charcot-Marie-Tooth neuropathy: clinical, electrophysiological, and morphological phenotype in four families with different connexin32 mutations. J Neurol Sci 1999;167:90–101. [PubMed: 10521546]

113. Sherratt RM, Bostock H, Sears TA. Effects of 4-aminopyridine on normal and demyelinated mammalian nerve fibres. Nature 1980;283:570–572. [PubMed: 7354839]

114. Söhl G, Willecke K. An update on connexin genes and their nomenclature in mouse and man. Cell Adhes Comm 2003;10:173–180.

115. Sorbo JG, Moe SE, Ottersen OP, Holen T. The molecular composition of square arrays. Biochemistry 2008;47:2631–2637. [PubMed: 18247481]

116. Spencer DF, Aryaeinejad R, Reber EI. Using the Cockroft-Walton voltage multiplier design in handheld devices. Nuclear Sci Symp Conf Record, 2001 IEEE 2001;2:746–749.

117. Stolinski C, Breathnach AS, Martin B, Thomas PK, King RHM, Gabriel G. Associated particle aggregates in juxtaparanodal axolemma and adaxonal Schwann cell membrane of rat peripheral nerve. J Neurocytol 1981;10:679–691. [PubMed: 6975804]

118. Stolinski C, Breathnach AS, Thomas PK, Gabriel G, King RHM. Distribution of particle aggregates in the internodal axolemma and adaxonal schwann cell membrane of rodent peripheral nerve. J Neurolog Sci 1985;67:213–222.

119. Suzuki H, Nishikawa K, Hiroaki Y, Fujiyoshi Y. Formation of aquaporin-4 arrays is inhibited by palmitoylation of N-terminal cysteine residues. Biochim Biophys Acta 2008;1778:1181–1189. [PubMed: 18179769]

120. Teubner B, Odermatt B, Güldenagel M, Söhl G, Degen J, Bukauskas FF, Kronengold J, Veselis VK, Jung YT, Kosak CA, Schilling K, Willecke K. Functional expression of the new gap junction gene connexin47 transcribed in mouse brain and spinal cord neurons. J Neurosci 2001;21:1117–1126. [PubMed: 11160382]

121. Uhlenberg B, Schuelke M, Ruschendorf F, Rug N, Kaindl AM, Henneke M, Thiele H, Stoltenburg-Didinger G, Aksu F, Topaloglu H, Hubner C, Weschke B, Gartner J. Mutations in the gene encoding gap junction protein alpha 12 (connexin 46.6) cause Pelizaeus-Merzbacher-like disease. Am J Human Genet 2004;75:251–260. [PubMed: 15192806]

122. Vanden Abeele F, Bidaux G, Gordienko D, Beck B, Panchin YV, Baranova AV, Ivanov DV, Skryma R, Prevarskaya N. Functional implications of calcium permeability of the channel formed by pannexin 1. J Cell Biol 2006;174:535–546. [PubMed: 16908669]

123. Verbavatz JM, Ma T, Gobin P, Verkman AS. Absence of orthogonal arrays in kidney, brain, and muscle from transgenic knockout mice lacking aquaporin-4. J Cell Science 1997;110:2855–2860. [PubMed: 9427293]

124. Wallraff A, Kohling R, Heinemann U, Theis M, Willecke K, Steinhauser C. The impact of astrocytic gap junctional coupling on potassium buffering in the hippocampus. J Neurosci 2006;26:5438–5447. [PubMed: 16707796]

125. Wang H, Kunkel DD, Martin TM, Schwartzkroin PA, Tempel BL. Heteromultimeric K+ channels in terminal and juxtaparanodal regions of neurons. Nature 1993;365:75–79. [PubMed: 8361541]

126. Waxman SG, Black JA. Freeze-fracture ultrastructure of the perinodal astrocyte and associated glial junctions. Brain Res 1984;308:77–87. [PubMed: 6434150]

127. White T, Paul D, Goodenough DA, Bruzzone R. Functional analysis of selective interactions among rodent connexins. Mol Biol Cell 1995;6:459–470. [PubMed: 7542941]

128. White TW, Bruzzone R. Multiple connexin proteins in single intercellular channels: connexin compatibility and functional consequences. J Bioenerg Biomemb 1996;28:339–350.

129. Wiley CA, Ellisman MH. Rows of dimeric-particles within glia, incorporated into a new model for the paranodal glia-axonal junction at the node of Ranvier. J Cell Biol 1980;84:261–280. [PubMed: 7380883]

130. Wingerchuk DM, Lennon VA, Lucchinetti CF, Pittock SJ, Weinshenker BG. The spectrum of neuromyelitis optica. Lancet Neurol 2007;6:805–815. [PubMed: 17706564]

131. Wolburg H. Orthogonal arrays of intramembrane particles: A review with special reference to astrocytes. J Brain Res 1995;36:239–258.

132. Wu C, Chang A, Smith MC, Won R, Yin X, Staugaitis SM, Agamanolis D, Kidd GJ, Miller RH, Trapp BD. 4 tubulin identifies a primitive cell source for oligodendrocytes in the mammalian brain. J Neurosci 2009;29:7649–7657. [PubMed: 19535576]

133. Yamamoto T, Ochalski A, Hertzberg EL, Nagy JI. LM and EM immunolocalization of the gap junctional protein connexin 43 in rat brain. Brain Res 1990;508:313–319. [PubMed: 2155040]

134. Yamamoto T, Ochalski A, Hertzberg EL, Nagy JI. On the organization of astrocytic gap junctions in the brain as suggested by LM and EM immunocytochemistry of connexin43 expression. J Comp Neurol 1990;302:853–883. [PubMed: 1964467]

135. Yamamoto T, Vukelic J, Hertzberg EL, Nagy JI. Differential anatomical and cellular patterns of connexin43 expression during postnatal development of rat brain. Dev Brain Res 1992;66:165–180. [PubMed: 1318799]

136. Yang B, Brown D, Verkman AS. The mercurial-insensitive water channel (AQP-4) forms orthogonal arrays in stably transfected CHO cells. J Biol Chem 1996;271:4577–4580. [PubMed: 8617713]

137. Young KC, Peracchia C. Opposite Cx32 and Cx26 voltage-gating to CO2 reflects opposite voltage-gating polarity. J Membr Biol 2005;202:161–170. [PubMed: 15798904]

138. Yu CS, Lin FC, Li KC, Jiang TZ, Zhu CZ, Qin W, Sun H, Chan P. Diffusion tensor imaging in the assessment of normal-appearing brain tissue damage in relapsing neuromyelitis optica. Am J Neuroradiol 2006;27:1009–1015. [PubMed: 16687534]

139. Zhou M, Xu G, Xie M, Zhang X, Schools GP, Ma L, Kimelberg HK, Chen H. TWIK-1 and TREK-1 are potassium channels contributing significantly to astrocyte passive conductance in rat hippocampal slices. J Neurosci 2009;29:8551–8564. [PubMed: 19571146]

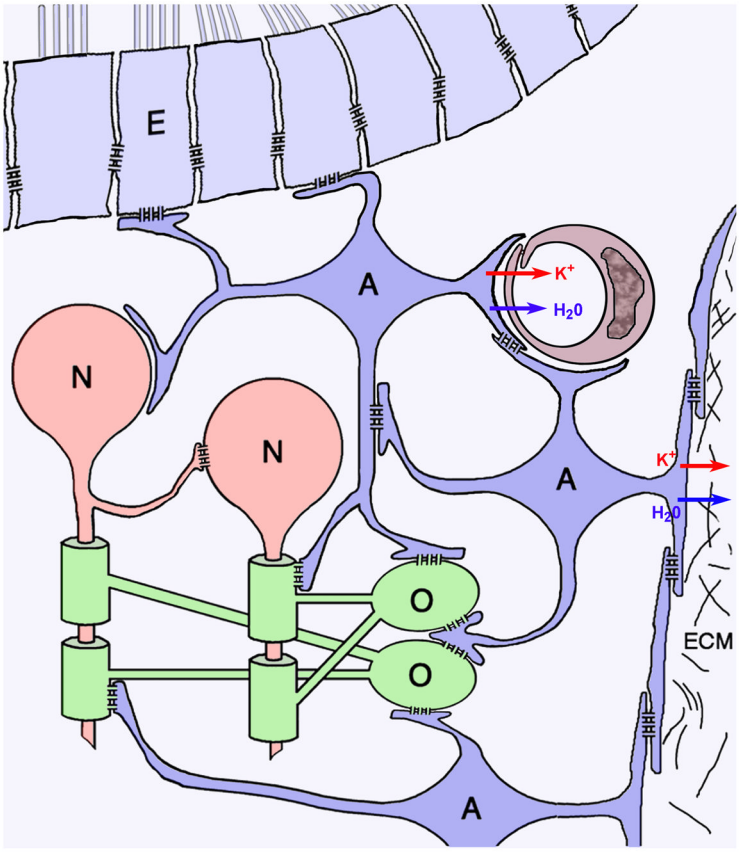

Fig. 1.

Cells of the panglial syncytium (astrocytes, *A, dark blue;* oligodendrocytes, *O, green;* ependymocytes, *E, light blue*) and their relationships to neurons (*N, red*), capillaries (*maroon*), and the glia limitans. Linked by abundant gap junctions, astrocytes act as "intermediaries" that couple oligodendrocyte somata, their "oligodendrite" processes, and their myelin segments to the astrocyte endfeet that surround capillaries and that form the glia limitans, where excess K^+ (*red arrows*) and osmotic water (*blue arrows*) are released into the circulatory system or into the bathing cerebrospinal fluid.

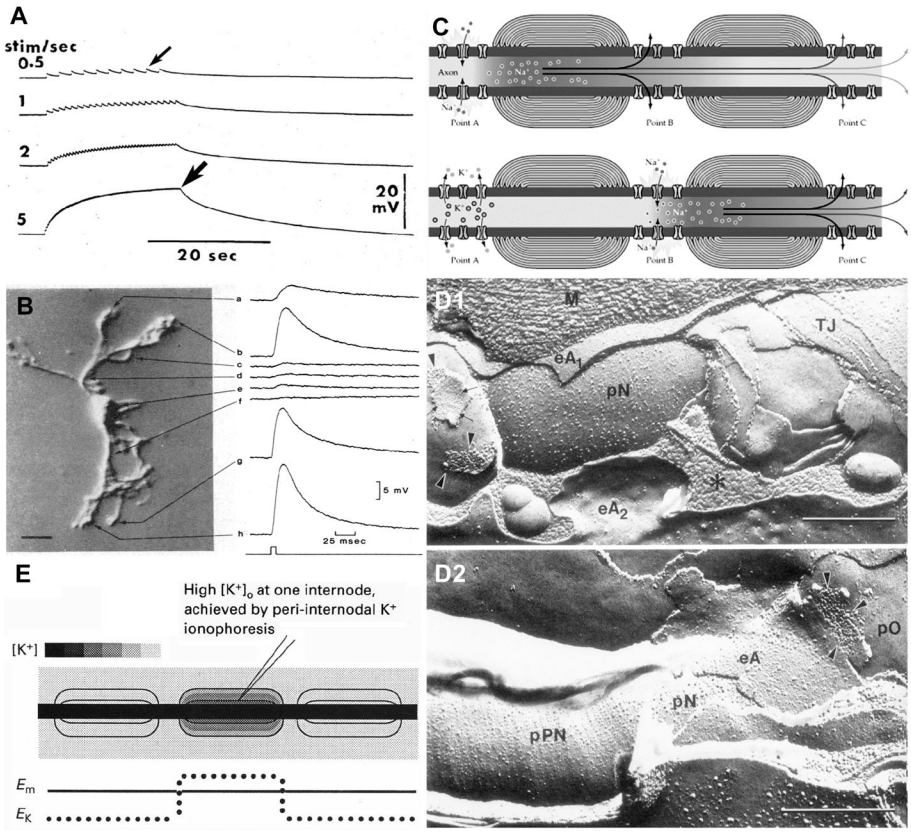

Fig. 2.

Evolution of concepts of K^+ movement associated with astrocytes at unmyelinated *vs.* myelinated axons. ***A)*** Depolarizations of distant astrocytes following stimulation of the distal end of unmyelinated axons in salamander optic nerve. At 0. 5 Hz, each depolarization causes a 0.5 mV depolarization (*small arrow*). At >5 Hz, cumulative depolarizations reach *ca.* 17 mV (*large arrow*), the approximate reversal potential of K^+. ***B)*** Focal application of high $[K^+]_O$ was detected as strong depolarizations (up to +15 mV) of the astrocyte endfeet (*traces a,b,g,h*) but as weak depolarizations of its soma and proximal processes (*traces c-f*). (From[81]; with permission). ***C)*** Typical textbook diagram indicating inward Na^+ current at nodes of Ranvier (*top*), followed 1 mSec later by outward K^+ current at the same node of Ranvier. (From[95]; with permission).) ***D)*** Association of astrocytes (eA2 in ***D1***, and eA in ***D2***) with nodes of Ranvier (pN) and with the paranodal surface of the axon (pPN in ***D2***). *Arrowheads* point to astrocyte-to-oligodendrocyte gap junctions on outer surface of myelin (***D1***, *left side;* ***D2***). ***E)*** Ultrasharp electrodes measured depolarizations of the "peri-internodal space" following each axonal action potential and following trains of action potentials. Each axonal action potential raised the potential of the peri-internodal space by several mV, with trains of action potentials raising the recorded voltage to +75 mV. (Estimated $[K^+]_P$ is as calibrated against *bar at upper left.*) Similar increases in K^+ were obtained by K^+ iontophoresis (from[29], with permission).

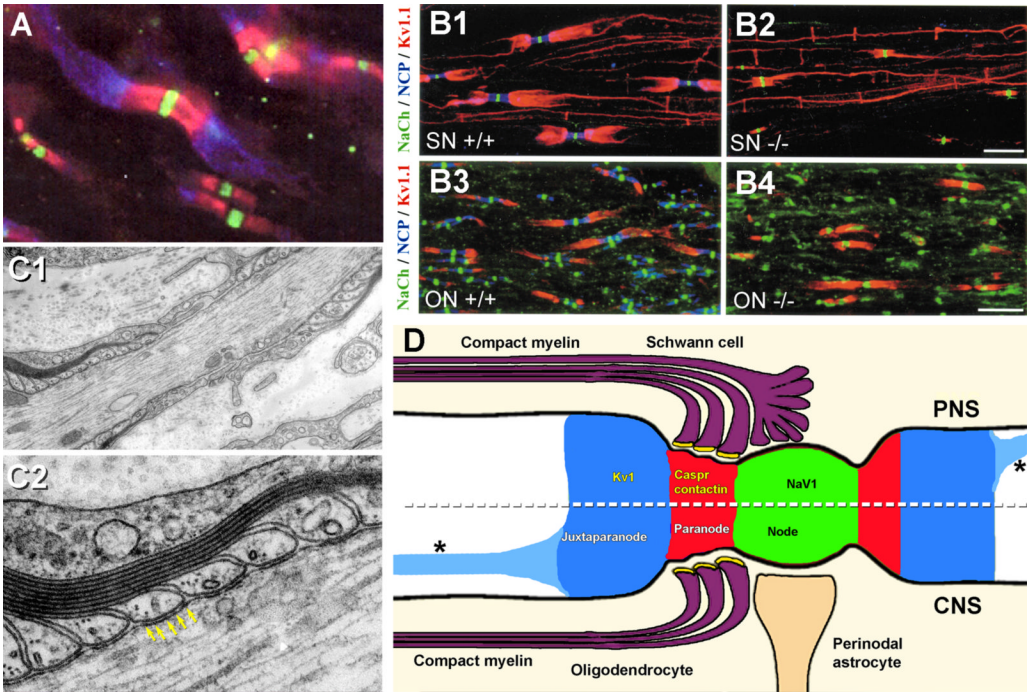

Fig. 3.

A) Immunofluorescence image demonstrating that Nav1 (v-g Na^+ channels) are present at nodes of Ranvier (*green* fluorescence), whereas Kv1 (v-g K^+ channels) are localized to the juxtaparanodal surface of the axons (*blue* fluorescence), with the two sets of channels segregated by membrane diffusion barriers established by contactin and contactin-associated proteins (caspr, *red*) associated with paranodal tight junctions. ***B)*** The Neurexin/contactin/paranodin barrier (*NCP; blue*) segregates Nav1 from Kv1.1 channels in both PNS sciatic nerve axons (*SN;* ***B1, B2***) and in CNS optic nerve axons (*ON;* ***B3, B4***). In the NCP knockout (−/−; ***B2*** and ***B4;*** *blue* fluorescence not present), Kv1 channels (*red*) migrate up to the NaV1 channels in the nodes (*green*) but do not intermix. Although densities of channels remain unchanged, saltatory conduction is reduced or destroyed in the -/- PNS and CNS axons. Note the thin line of Kv1.1 channels linking from juxtaparanode to juxtaparanode in the PNS (***B1, B2***) but only faintly resolvable in the much smaller CNS axons (***B3, B4***). ***C)*** Thin-section TEM image of paranodal loops of myelin, which are linked to the axon by “septate junctions” (*yellow arrows*) that are composed of contactin and caspr (from100). ***D)*** Drawing showing distributions of Nav1, Kv1.1 and contactin/caspr in PNS (*above dotted line*) and CNS (*below dotted line*). A pathway for K^+ from peri-internodal space to astrocytes is not specified. [Redrawn from18·97; with permission.] Asterisks (*), K^+ channels along the inner mesaxon (from14).

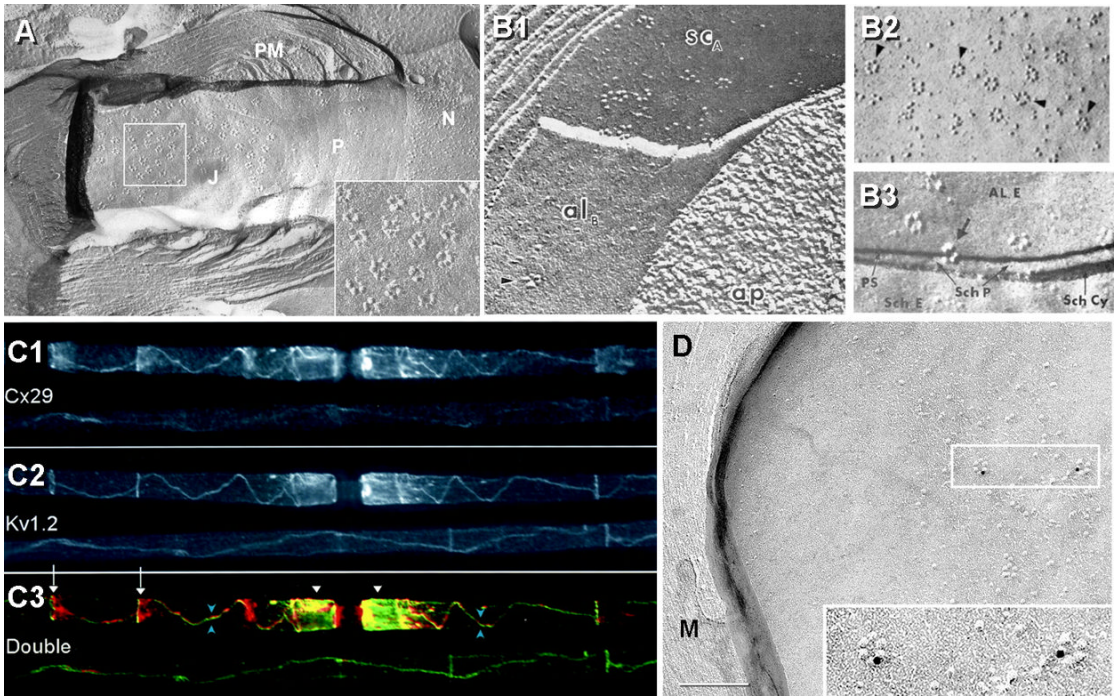

Fig. 4.

Axonal and myelin rosettes correlated with Kv1.2 and Cx29, respectively. ***A)*** E-face image of axon plasma membrane, revealing the node of Ranvier *(N)*, its contiguous paranodal surface *(P)* and juxtaparanodal surface *(J)*. Terminal loops of paranodal myelin *(PM)* contact the axon, forming shallow grooves representing imprinted paranodal junctions [129]. Axonal E-face rosettes are concentrated in the juxtaparanodal membrane, but a few are between paranodal imprints (above the *P*). Inset; higher magnification view of 16 rosettes. (From *Electrophorus electricus;* unpublished image courtesy of Dr. Nancy Shinowara, NIH.) ***B1)*** E-face rosettes in the axonal plasma membrane (*yellow arrow*) and P-face rosettes in the innermost layer of Schwann cell myelin (***B1*** from[67]; ***B2-B3*** from117,118). ***B2)*** Rosettes are abundant in innermost myelin juxtaparanodal P-face. ***B3)*** Fractures from axonal E-face to innermost myelin P-face reveal that the rosette IMPs are aligned from axon to myelin plasma membrane, demonstrating tight structural coupling and implying functional coupling. ***C1-C3)*** Co-localization of Cx29 (***C1***) and Kv1.2 (***C2***) at juxtaparanodes and along the inner mesaxon, from juxtaparanode to juxtaparanode (overlay in ***C3***), precisely where the rosettes occur in axonal and myelin adaxonal plasma membranes. ***D)*** By FRIL, Cx29 was localized to P-face rosettes on innermost juxtaparanodal myelin (two rosettes labeled for Cx29 by 10-nm gold beads are shown in inset). No connexin coupling partner for Cx29 is present in the internodal segment, but Kv1 channels are co-localized in the axonal plasma membrane.

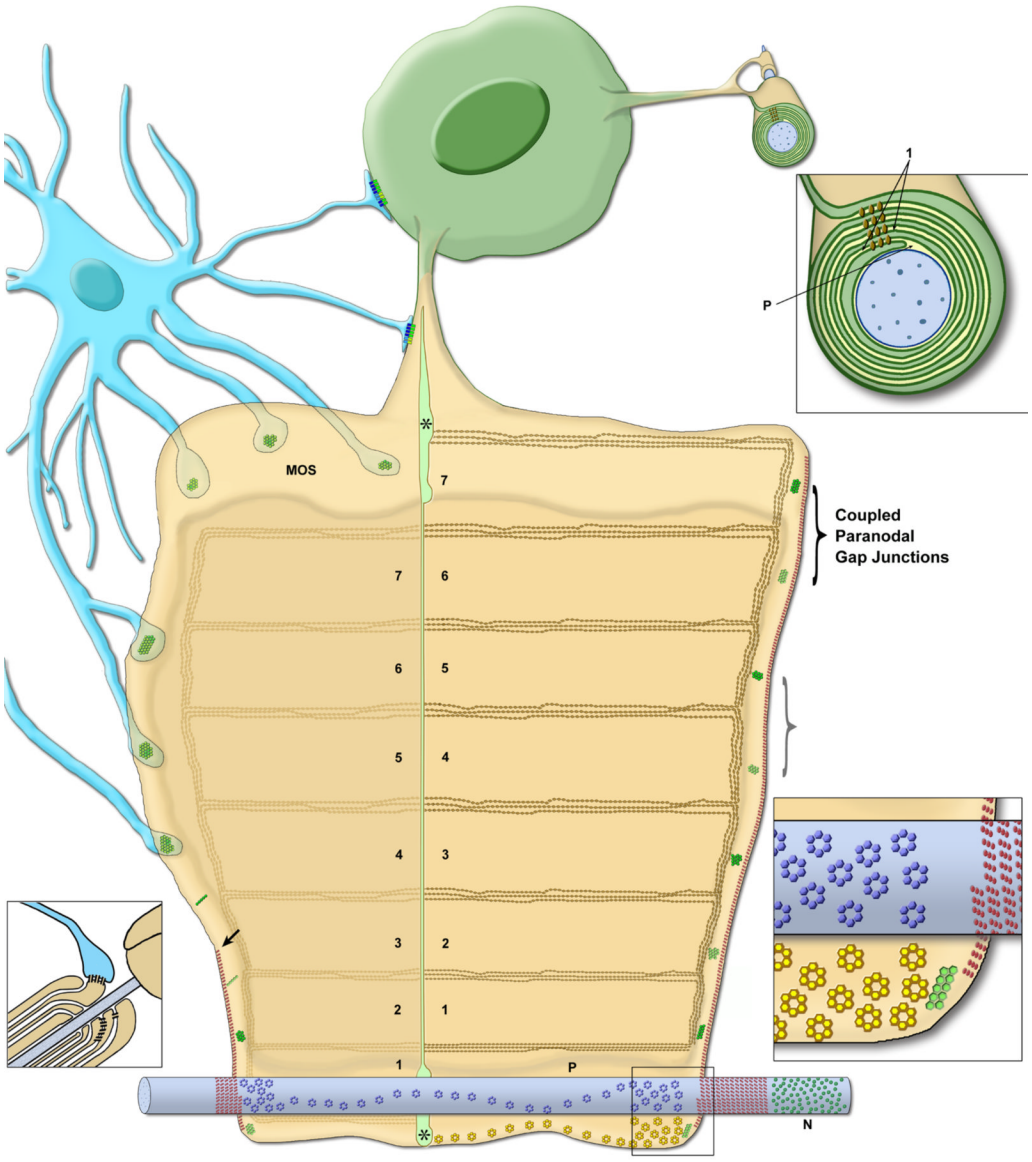

Fig. 5.

Diagram of one segment of oligodendrocyte myelin, unrolled to show molecular specializations of both inner (adaxonal, *right side*) and outer (abaxonal, *left side*) surfaces.. The oligodendrocyte soma (*green*) is connected by oligodendrites to many different myelin segments. An astrocyte (*blue)* has processes that form gap junctions with the abaxonal surface of myelin, including on everted paranodal loops *(left side* and *left inset)*. #1-#7, intra-myelin extracellular spaces, separated by tight junctions; *asterisks*, cytoplasm in innermost and outermost cytoplasmic tongues of myelin; *arrow*, termination of septate junction at first everted paranodal loop; *blue cylinder*, axon; *blue rosettes*, Kv1 channels in the axon internodal plasma membrane, concentrated at the juxtaparanodal surface and along the inner mesaxon; *brackets*, paired Cx32-containing gap junctions linking the abaxonal to the successively more external adaxonal surface; *brown diamonds in lines*, tight junction strands on myelin abaxonal surface *(light lines)* to those on the next outward adaxonal surface *(dark lines); green IMPs in hexagonal arrays and lines*, Cx32-containing gap junctions between paranodal loops of myelin,

either as small plaque or string gap junctions; *greenish-yellow-hexagonal arrays*, Cx32/Cx47 to Cx30/Cx43 heterotypic heterologous gap junctions; *N*, nodal extracellular space; *P*, peri-axonal internodal extracellular space; *triplet red ovals as dotted line*s, septate junctions binding the paranodal loops to the axon plasma membrane, forming a spiral barrier separating the nodal extracellular space from the peri-internodal extracellular space; *yellow rosettes*, Cx29 intramembrane particles in innermost adaxonal myelin; *left inset*, longitudinal section of everted paranodal loops; *lower right inset*, detailed view of the Kv1.1 and Cx29 rosettes in the juxtaparanodal region, adjacent to the septate junction barrier (represented as *triplet red IMPs*); upper right inset, cross-sectional view of myelin, *1*, first intra-myelin extracellular space, between the innermost two sets of tight junction strands (*brown diamonds*); *P*, peri-internodal space;.

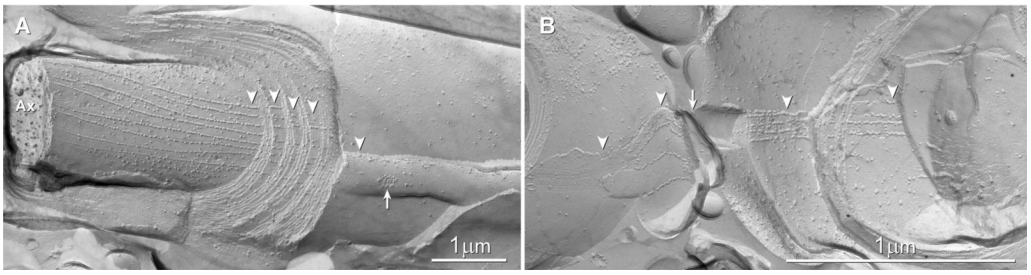

Fig. 6.

A, B Intralamellar tight junctions. ***A)*** Multiple tight junction strands stacked from outer mesaxon to inner mesaxon separate each layer of internodal myelin extracellular space into ionically and electrically-distinct compartments, one per layer of myelin wrapping. *Arrow*, outer tongue of myelin. ***B)*** Tight junctions of two adjacent myelinated fibers are aligned from outer tongue to outer tongue (*arrow*), making these linked cross-fractured axon pairs resemble a “figure 8”. *Arrowheads*, tight junctions; *Ax*, axon cytoplasm. *Scale bars*, 1 μm.

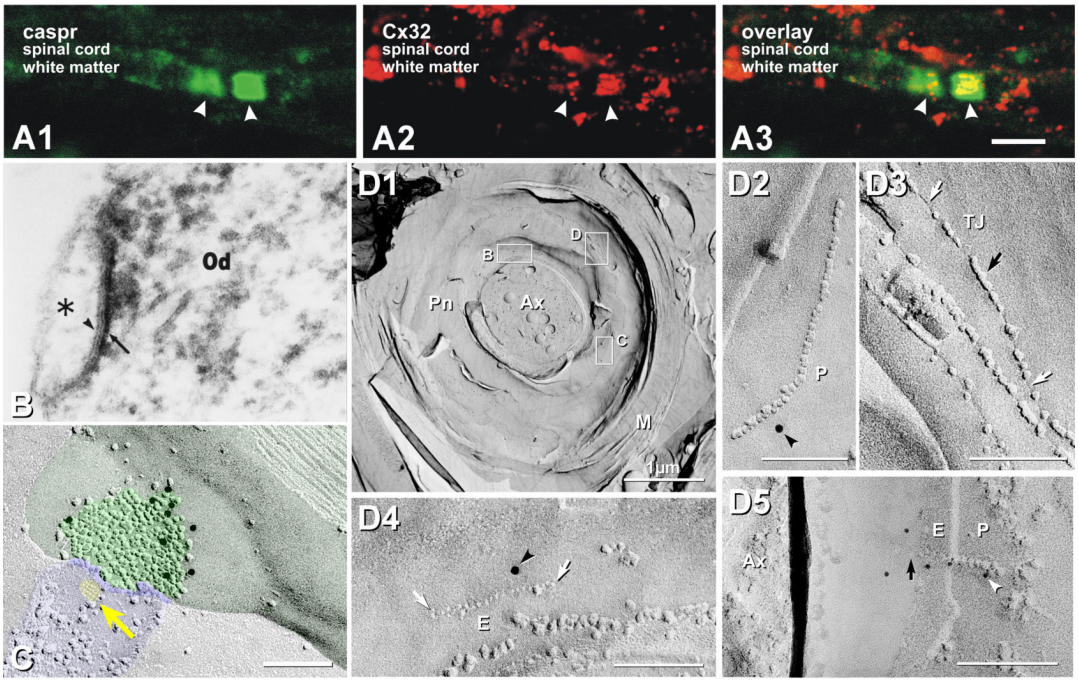

Fig. 7.

Co-association of Caspr and Cx32 in paranodal myelin. ***A)*** Immunolabeling for caspr (*green*) occurs only at paranodes, whereas labeling for Cx32 (*red*) frequently occurs within paranodal myelin. ***B)*** Thin section TEM image of astrocyte/oligodendrocyte gap junction labeled for Cx32 by immunoperoxidase [from[54], with permission]. ***C)*** Astrocyte-to-oligodendrocyte (A:O) gap junctions, with the astrocyte process identified by the imprint of an AQP4 "square array" *(yellow arrow)* linked by a gap junction to the outer surface of myelin. The gap junction consists of multiple clusters of hexagonally-arranged 9-nm particles in the otherwise relatively smooth outermost layer of myelin60›69. Nine 10-nm gold beads label Cx32 (from45). ***D1)*** Cx32 in "string" gap junctions link successive paranodal loops. Gap junctions consist of 9-nm IMPs in P-faces ***(D2, D5)*** and/or 9-nm pits in E-faces ***(D4, D5)***, both of which are labeled for Cx32 by 12-nm (***D2, D4***) and 6-nm gold (***D5***). In such formaldehyde-fixed tissue, tight junctions ***(D3)*** consist of mixed IMPs and pits on both P- and E-faces (*black vs. white arrows*), whereas gap junctions consist of 100% P-face IMPs and 100% E-face pits. Note grooves (linear pits) linking paranodal tight junction IMPs (**D3,** *white vs. black arrows*; from45).

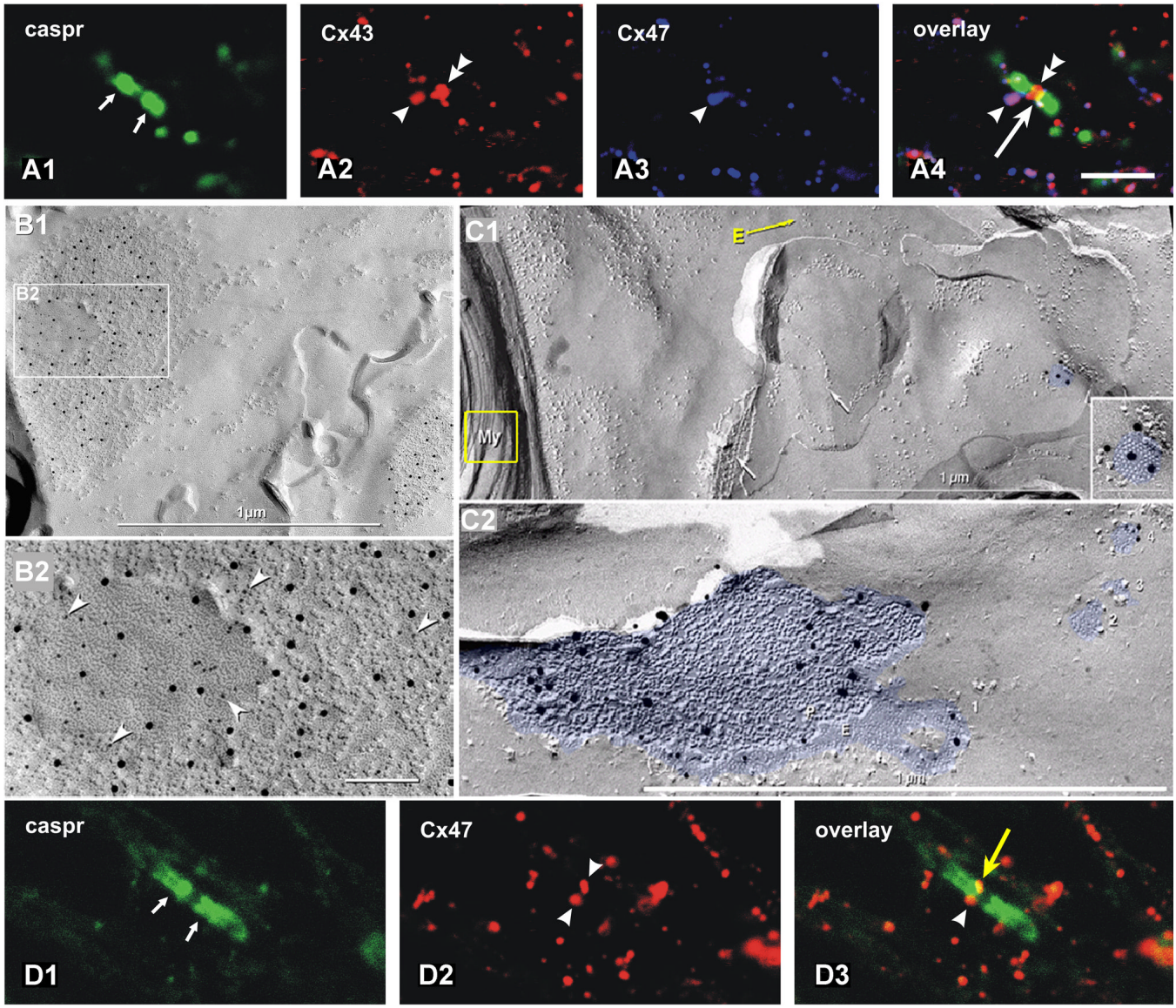

Fig. 8.

Co-localization of Cx43 and Cx47 at A:O gap junctions, triple co-localization with caspr at paranodes. ***A1-A4)*** Triple-immunofluorescence labeling for caspr (*green, small arrows*), Cx43 (*red, arrowheads*) and Cx47 (*blue, arrowhead*). *Purple*, co-localization of Cx43 and Cx47; *white, large arrowhead*, triple co-localization of caspr, Cx43 and Cx47. ***B1, B2)*** Gap junctions on oligodendrocyte soma, double-labeled for Cx32 (6-nm gold beads, *arrowheads*) and Cx47 (12-nm gold beads). Both connexins are present in >90% of heterologous O:A gap junctions, whether on the soma, their "oligodendrites" or on the surface of myelin. [From[45].] ***C1, C2)*** Gap junctions linking the outer layer of myelin with astrocytes, identified because they are labeled for astrocyte-specific connexins. The connexins of the attached cell are single-labeled for Cx43 (*20 nm gold* in ***C1***) and double-labeled for Cx43 *(10-nm gold* in ***C2***) and Cx30 (*20-nm gold* in ***C2***). ***C1)*** The yellow arrow at "E" traces continuity from cross-fractured myelin (*yellow box)* to areas containing Cx43-labeled gap junction (enlarged in inset). ***C2)*** Large oligodendrocyte E-face to astrocyte P-face (O:A) gap junction on outer layer of myelin; labeled for both Cx30 and Cx43. Two small gap junctions are unlabeled. ***D1-D3)*** Double- labeling for

caspr (*green*) is localized to paranodal loops of myelin, whereas labeling for Cx47 (*red*) defines the presence of oligodendrocyte Cx47. Overlay reveals that Cx47 is present on the shoulders of the paranodal loops, presumably within gap junctions linking successive paranodal loops.

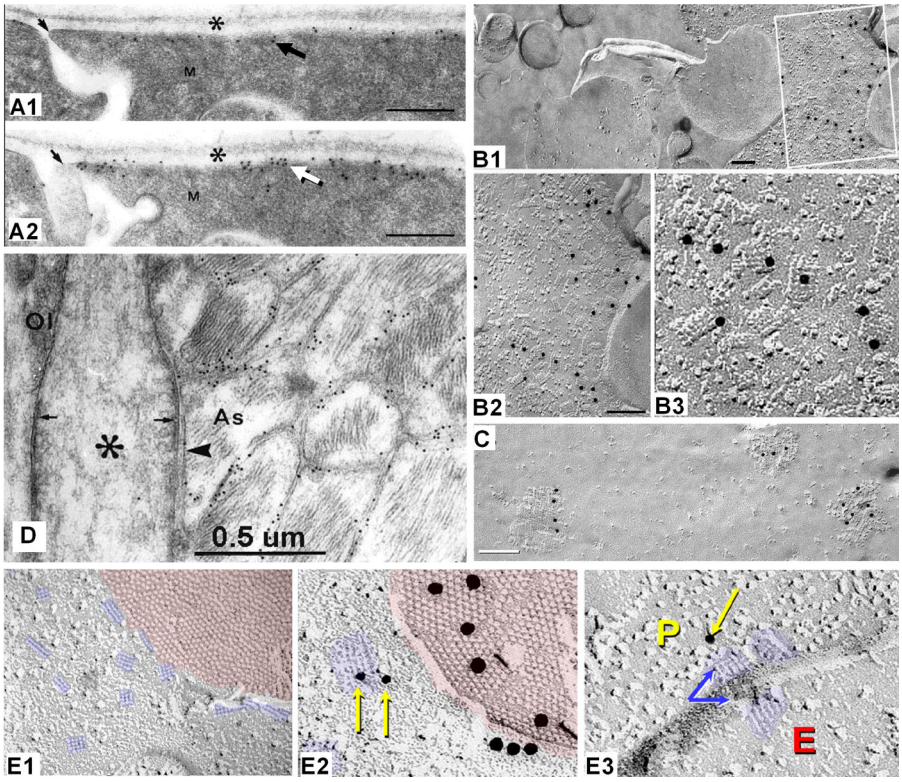

Fig. 9.

Localization of Kir4.1 and AQP4, and association of AQP4 with astrocyte gap junctions. ***A1, A2)*** Consecutive ultrathin sections immunogold labeled for Kir4.1 (***A1***) and AQP4 (***A2***), demonstrating intermixing of proteins. *Asterisk* (*), vitreal surface of the retina; *M*, Müller cell endfeet. Scale bars = 0.25 μm. [From70]. ***B1-B3)*** FRIL identification of AQP4 in "square arrays" in astrocyte endfeet at the pia/glia limitans (from107). Immunogold beads (*arrow*) label *ca.* 35% of "square arrays". *Box* in ***B1*** enlarged as ***B2. C)*** CHO cells in which M23 arrays are immunogold labeled for AQP4. ***D)*** Node of Ranvier and surrounding astrocyte processes, labeled for AQP4 (*10-nm immunogold beads*). Gold beads follow the outlines of all astrocyte processes except at the area of contact with the nodal plasma membrane (*arrowhead*). Nodal thickenings (*small arrows*; from72). Astrocytes contain dense bundles of GFAP filaments. ***E1-E3)*** AQP4 arrays often cluster around ependymocyte (***E1, E2)*** and astrocyte and gap junctions. By FRIL ***(E1-E3)***, square arrays are labeled for AQP4 (*10-nm gold*), whereas the ependymocyte gap junction is labeled for Cx43 (*20nm gold*, ***E2***).

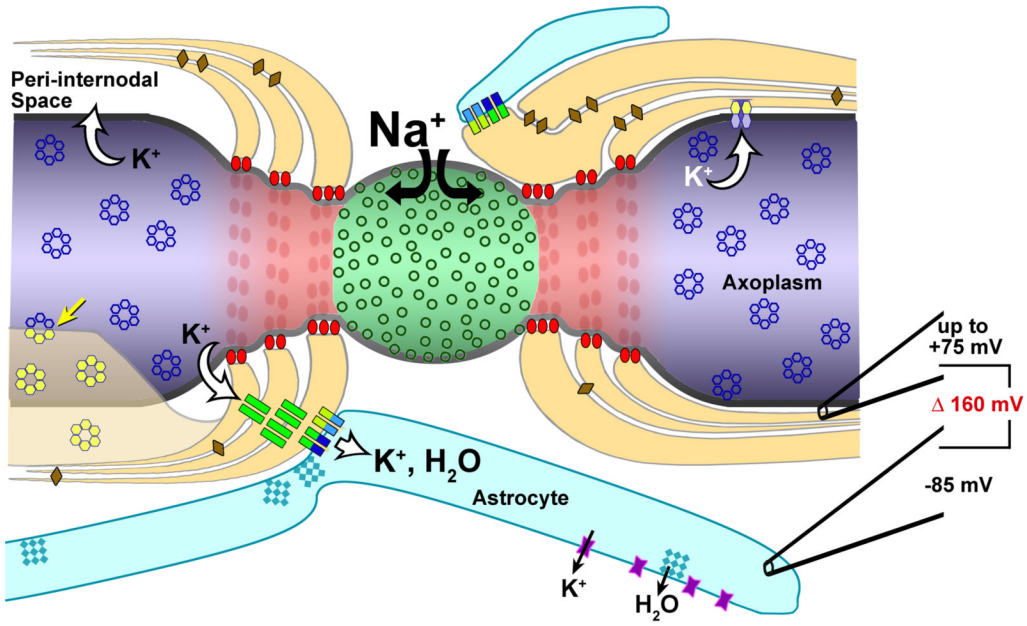

Fig. 10.

Locations of principal proteins identified to date at nodes of Ranvier, paranodes, and juxtaparanodes. Nav1 channels, *green circles* in *green node of Ranvier*. *purple hour-glass particles*, Kir4.1; *blue rosettes*, possible Kv1 channels in juxtaparanodal membrane (*blue*); *dark blue connexons*, Cx30; *dark green connexons*, Cx32; *light blue connexons*, Cx43; *red ovals*, caspr/contactin septate junctions in paranodal membrane (*red*); *teal square lattices*, AQP4; *yellow-green connexons*, Cx47; *yellow rosettes*, Cx29 in PNS myelin[57]. Fracturing from innermost myelin to the axon plasma membrane (*yellow arrow*) revealed that the rosettes are structurally coupled from myelin to axon plasma membrane (see Fig. 4B3). Note the 160 mV difference in electrical potential between the peri-internodal compartment (*upper electrode*, right side of drawing) and the astrocyte cytoplasm (*lower electrode*), measured using "ultra-sharp" recording electrodes[28,29].

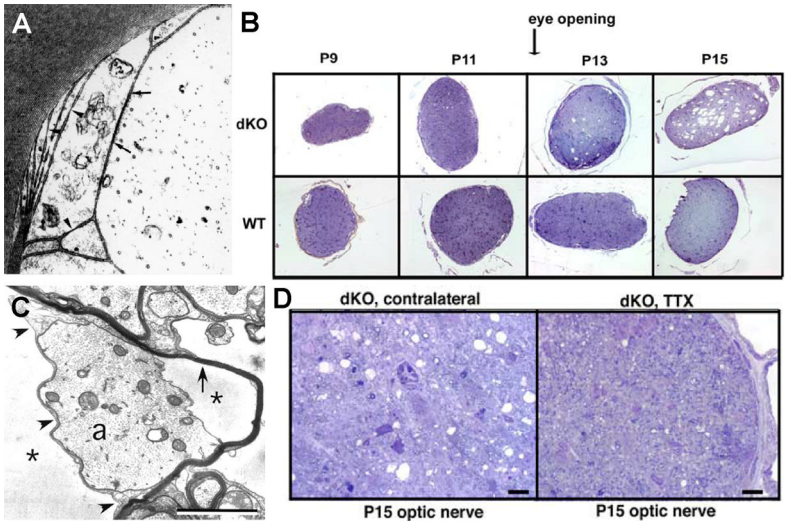

Fig. 11.

Effects of mutation/deletion of Cx32 and Cx47. ***A)*** Separation of inner layers of myelin in CMTX indicate that K^+ and H_2O enter inner myelin layers without compensatory transport to outer layers or to astrocytes (from112). ***B)*** Effects of increased axonal activity on myelin in Cx32/Cx47 double knockout animals. Cross-sections of Cx32/Cx47 dKO mouse optic nerve (*upper panel*) and comparison to optic nerve in age-matched wildtype mice (*lower panel*). Following eye opening (P11) and increased axonal activity, myelin is vacuolated in the dKO animals but remains normal in the wildtype (WT). Vacuolation began at *ca.* P13 in dKO mice but did not occur in WT (from65). ***C)*** Thin-section transmission electron micrograph showing swollen cytoplasm in innermost layer of myelin (*left side*) and separation of adaxonal myelin from axon (*right side*), consistent with excess K^+ and H_2O in the peri-internodal space (from65). ***D)*** Cx32/Cx47 dKO mice in which one retina was exposed to TTX (*right side*), thereby blocking all retinal axonal saltatory conduction, decreased axonal activity resulted in reduced myelin swelling as compared with the uninjected contralateral side (*left image*; from65).

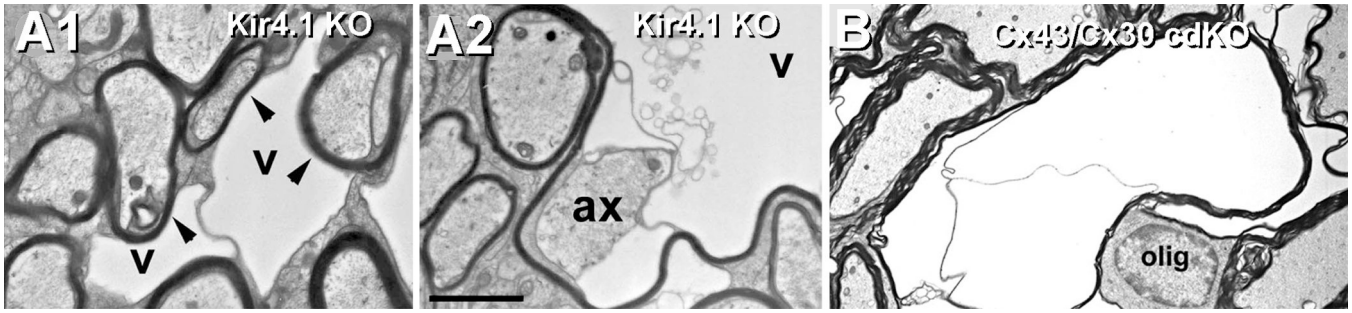

Fig. 12.

Effects of molecular disruption of Kir4.1 *vs.* double knockout of Cx43/Cx30 in astrocytes. ***A)*** As occurred in Cx32/Cx47 dKO mice (Fig. 11), the innermost layer of myelin is enlarged or swollen in Kir4.1 KO mice, presumably by excess K^+ and accompanying osmotic water. Note that separation of inner and outer layers of myelin (***A1***) and that large vacuoles (***A2***) are present in the innermost layer of myelin, immediately adjacent to the axon plasma membrane. From[66]. ***B)*** Similar swelling and vacuolation of myelin is also seen in Cx30/Cx43 conditional double-knockout mice in which the expression of the cdKO is restricted to astrocytes[124]. Thus, disruption of several diverse pathways for K^+ and H_20 handling in the panglial syncytium result in myelin swelling and necrosis.

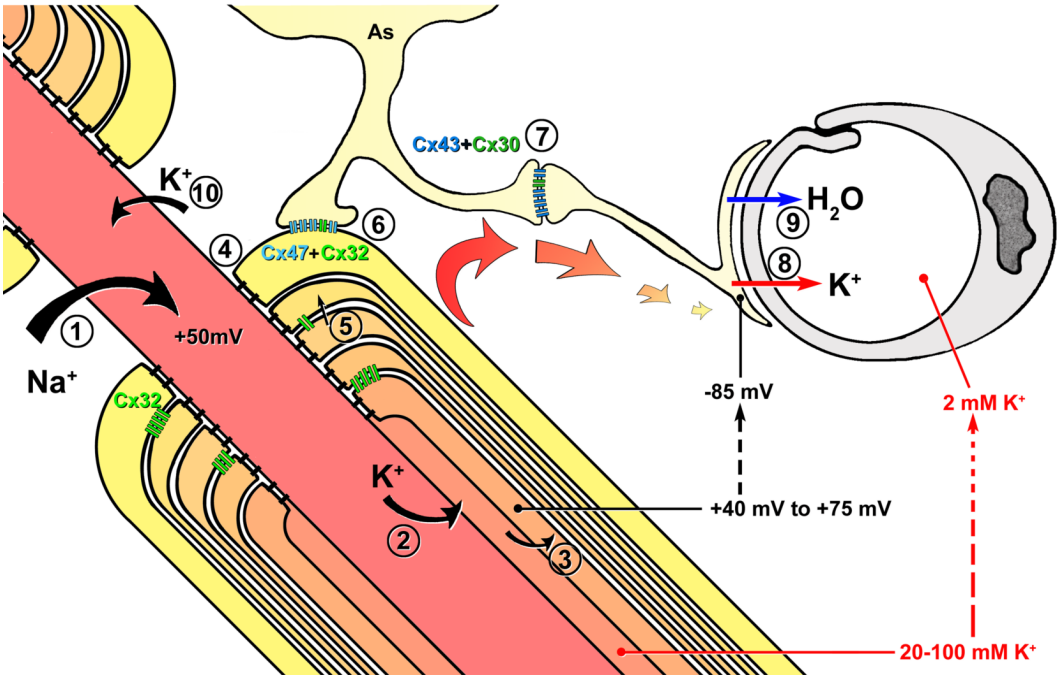

Fig. 13.

Diagram depicting entry of Na^+ at nodes of Ranvier, exit of K^+ at juxtaparanodal axonal plasma membrane, and intracellular and intercellular pathways for both K^+ and H_2O through Cx32-gap junctions linking successive layers of myelin, into the astrocyte syncytium via bi-heterotypic (Cx47/Cx32:Cx43/Cx30) gap junctions, and ultimately to the astrocyte endfeet. Relative K^+ concentrations at each intracellular location are indicated by progressive changes in intensity of *orange* to *light yellow*. Note the relative differences in recorded electrical potentials (+75 to -85 mV) (and tonicity (20-100 mM K^+ in peri-internodal space to 2 mM K^+ in capillary lumen). Modified from[45].